2012

The Demonstration of SMSE Based Cognitive Radio in Mobile Environment via Software Defined Radio

Ruolin Zhou
Wright State University

The Demonstration of SMSE Based Cognitive Radio in Mobile Environment via Software Defined Radio

A dissertation submitted in partial fulfillment
of the requirements for the degree of
Doctor of Philosophy

by

Ruolin Zhou
M.S.Egr., Wright State University, 2007
B.E., Dalian Railway Institute, China, 2003

2012
Wright State University

Wright State University
GRADUATE SCHOOL

November 4, 2011

I HEREBY RECOMMEND THAT THE DISSERTATION PREPARED UNDER MY SUPERVISION BY Ruolin Zhou ENTITLED The Demonstration of SMSE Based Cognitive Radio in Mobile Environment via Software Defined Radio BE ACCEPTED IN PARTIAL FULFILLMENT OF THE REQUIREMENTS FOR THE DEGREE OF Doctor of Philosophy.

Zhiqiang Wu, Ph.D.
Dissertation Director

Ramana V. Grandhi, Ph.D.
Director, Ph.D. in Engineering Program

Andrew Hsu, Ph.D.
Dean of Graduate School

Committee on
Final Examination

Dr. Zhiqiang Wu

Dr. Henry Chen

Dr. Ryan Thomas

Dr. Yong Pei

Dr. Yan Zhuang

ABSTRACT

Zhou, Ruolin. Ph.D., Engineering Ph.D. Program, College of Engineering and Computer Science, Wright State University, 2012.
The Demonstration of SMSE Based Cognitive Radio in Mobile Environment via Software Defined Radio.

With the emergence of increasing number of wireless devices and demands for higher data rates, spectrum crowding and congestion increases. Spectrum congestion problem has been challenging wireless communication engineers for a few decades. However, recent studies indicate that most of the time wide ranges of the radio spectrum are rarely utilized. Hence, the spectrum congestion is mainly due to the inefficient spectrum usage rather than the spectrum scarcity. To exploit under used spectrum and utilize the spectrum efficiently in dynamically changing environments, a new technology is needed. Cognitive Radio (CR) arises to be a possible solution to spectral crowding problem by introducing the opportunistic usage of frequency bands that are not heavily occupied by licensed users.

In this dissertation, we implement and demonstrate an autonomous cognitive radio system in mobile environment via SDR. We first design and implement an intelligent spectrum sensing engine which can detect the existence of the primary user (PU) signal and accurately estimate its radio frequency (RF) parameters. Second, with the aid of the spectrum sensing engine, a spectrum mask is provided. Meanwhile, a multi-carrier waveform is generated based on spectrally modulated spectrally encoded (SMSE) framework. With the dynamic multi-carrier non-contiguous waveform, an intelligent interference avoidance SMSE-based cognitive radio is implemented and demonstrated using universal software radio peripheral (USRP) and GNU software defined radio (SDR) platform. Third, we propose a novel total intercarrier interference (ICI) cancellation scheme to eliminate the ICI in mobile environment, apply the algorithm to the SMSE base cognitive ra-

dio, employ GNU SDR platform and USRP, implement and demonstrate an SMSE based cognitive radio in high mobility environment. Combined with the spectrum sensing engine, the cognitive radio is capable of detecting the availability of each and every subcarrier in the operational bandwidth. By turning off those subcarriers occupied by the primary users, the cognitive radio implements a non-contiguous SMSE transmission waveform. Integrated with total ICI cancellation algorithm, the cognitive radio has the ability to eliminate the ICI due to the frequency offset caused by mobility.

There are a few unique features of our cognitive radio implementation: (1) we have demonstrated real-time seamless video transmission without interference to primary users, and without interference from primary users; (2) our cognitive radio is capable of taking advantage of multiple spectrum holes and operating over multiple non-contiguous spectrum bands (our demonstration is the first in the world to stitch multiple non-contiguous spectrum holes together); (3) the cognitive radio dynamically adjusts which subcarriers to turn off according to the primary users' transmission; (4) the cognitive radio can also adjust other parameters such as the total number of subcarriers, center frequency, and bandwidth of each subcarrier; (5) the cognitive radio maintains all the features even in high mobility environment, making it a flexible, agile, and robust cognitive radio node in mobile communication system.

Contents

List of Figures

List of Tables

Introduction

1.1 Motivation

'Spectrum is the lifeblood of Radio Frequency (RF) Communications' [1]. With the emergence of increasing number of wireless devices, and the demands for higher data rates, spectrum congestion problem increases. However, recent studies have characterized that the spectrum congestion is mainly due to the inefficient spectrum usage rather than the spectrum scarcity [2]. Dynamic spectrum access (DSA) [3] and cognitive radio (CR) [4] have been emerging to utilize the frequency spectrum in an efficient and opportunistic manner.

To exploit under used spectrum and utilize the spectrum efficiently in dynamically changing environments, CR [4] has been considered as a strong candidate for next generation wireless communication. In previous work of the Broadband, Mobile and Wireless Networking Laboratory at Wright State University, researchers have proposed and demonstrated a cognitive centric overlay/underlay waveform design through a spectrally modulated spectrally encoded (SMSE) framework to improve the bit error rate (BER) performance and network throughput of a cognitive radio [5][6][7]. In this dissertation, we extend this work to use software defined radio to implement the cognitive centric overlay waveform in [5][6][7] and demonstrated an adaptive interference avoidance overlay cognitive radio in static

environment and highly mobile environment.

In mobile radio channels, the orthogonality among subcarriers of SMSE overlay waveforms is lost due to the frequency offset caused by mobility. As a direct result, intercarrier interference (ICI) is observed on each and every subcarrier, leading to significant performance degradation. We propose a novel total ICI cancellation algorithm for SMSE waveforms in mobile communication system to eliminate the ICI entirely without lowering the transmission rate nor reducing the bandwidth efficiency. Specifically, the total ICI cancellation scheme takes advantage of the orthogonality of the ICI coefficient matrix and offers perfect ICI cancellation and significant BER improvement at linearly growing cost. We also integrate the total ICI cancellation in our SDR based implementation and demonstration of cognitive radio.

We first design and implement an intelligent spectrum sensing engine for cognitive radio network, which can detect the existence of the primary users and accurately estimate their RF parameters. Second, with the aid of the intelligent spectrum sensing engine, a spectrum mask is provided. With a multi-carrier waveform generated from SMSE framework, an intelligent interference avoidance SMSE-based cognitive radio is implemented and demonstrated using universal software radio peripheral (USRP) and GNU software defined radio (SDR) platform. Third, we implement the total ICI cancellation scheme to eliminate ICI and improve the performance in high mobility environment. Specifically, we employ the SMSE framework to generate multi-carrier transmission waveforms over multiple non-contiguous frequency bands. Combined with the spectrum sensing engine, the cognitive radio is capable of detecting the availability of each and every subcarrier in the operational bandwidth accurately. By turning off those subcarriers occupied by the primary users, the cognitive radio implements non-contiguous SMSE transmission. Integrated with total ICI cancellation algorithm, the cognitive radio has

the ability to eliminate the ICI due to the frequency offset caused by mobility.

There are a few unique features of our cognitive radio implementation: (1) we have demonstrated real-time seamless video transmission without interference to primary users, and without interference from primary users; (2) our cognitive radio is the first in the world to take advantage of multiple spectrum holes and operating over multiple non-contiguous spectrum bands; (3) the cognitive radio dynamically adjusts which subcarriers to turn off according to the primary users' transmission; (4) the cognitive radio can also easily adjust other parameters such as the total number of subcarriers, center frequency, and bandwidth of each subcarrier; (5) the cognitive radio maintains all the features even in high mobility environment by using total ICI cancellation, making it a flexible, agile, and robust cognitive radio node in mobile environment.

1.2 Overview of Cognitive Radio

Fig. 1.1 [8] shows the radio frequency spectrum allocation in US. It clearly shows the spectrum congestion problem facing wireless service providers and wireless communication engineers. However, recent research characterizing the actual spectrum usage by DARPA's XG program indicates that only up to 6% of the spectrum is being utilized at a given time. Fig. 1.2 [2] shows the signal strength distribution over a large portion of the spectrum. Hence, the reason of the spectrum congestion revealed by these measurements is not mainly due to the spectrum scarcity, but the inefficient spectrum utilization.

Cognitive radio (CR) and dynamic spectrum access (DSA) have been proposed to solve current spectrum inefficiency problems and increase the utilization of the spectrum. CR is an intelligent radio which is capable of setting and configuring its own parameters including 'waveform, protocol, transmitting and receiving

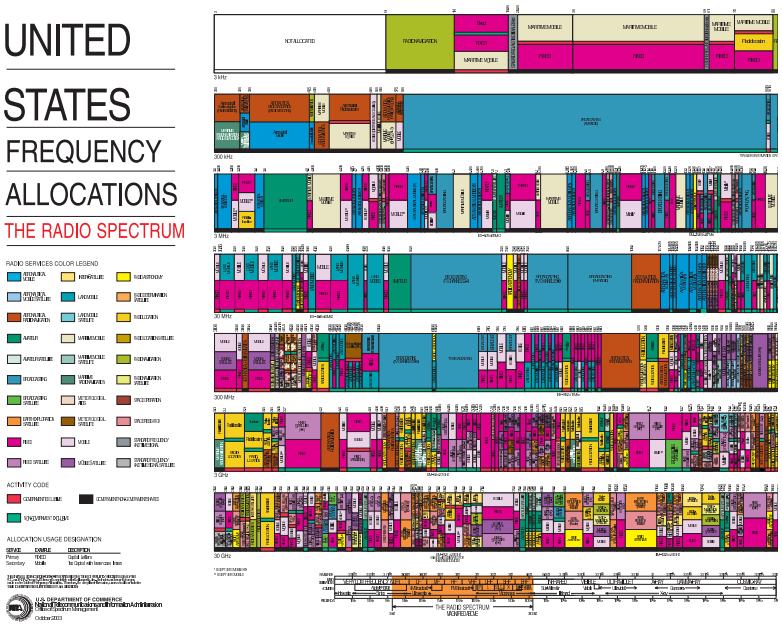

Figure 1.1: Spectrum Allocation

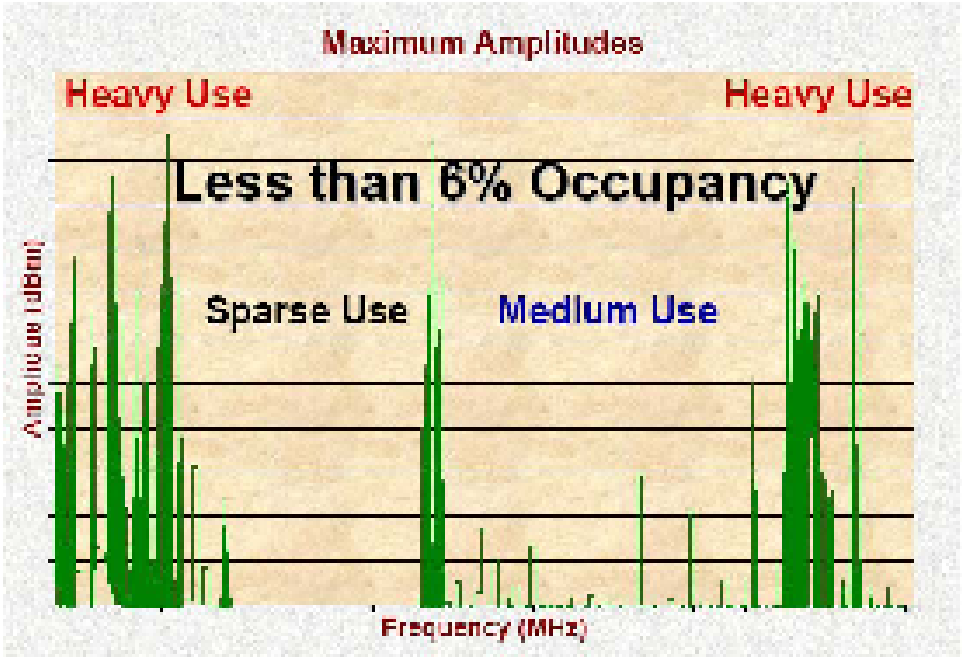

Figure 1.2: Actual Spectrum Utilization

carrier frequency and networking' autonomously [4]. The cognition cycle defined by Mitola in [4] is shown in Fig. 1.3. Specifically, CR system has the ability of sensing, learning and adapting so that it is the main technology enabler for DSA. Chakravarthy simplified the cognition cycle in [9] which is shown in Fig. 1.4

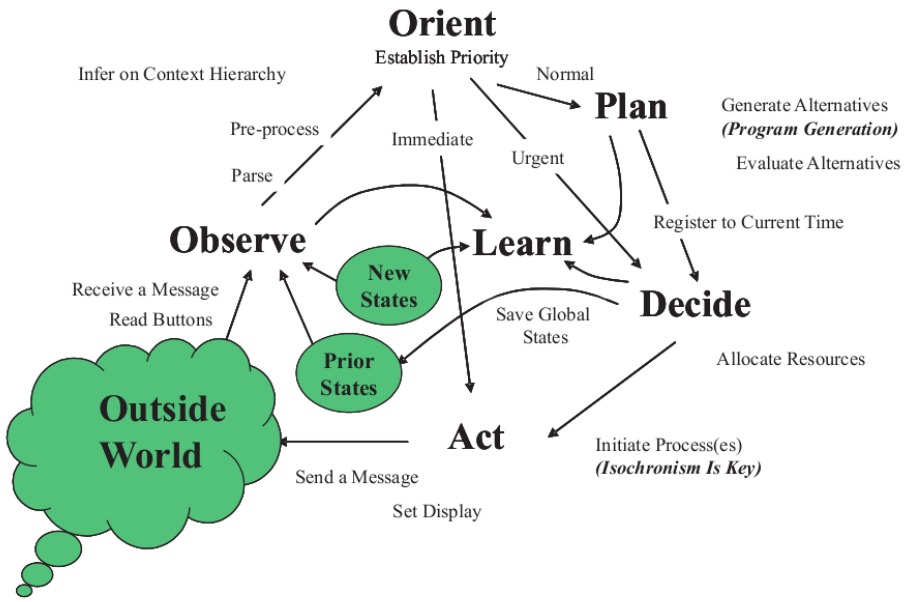

Figure 1.3: Cognition Cycle

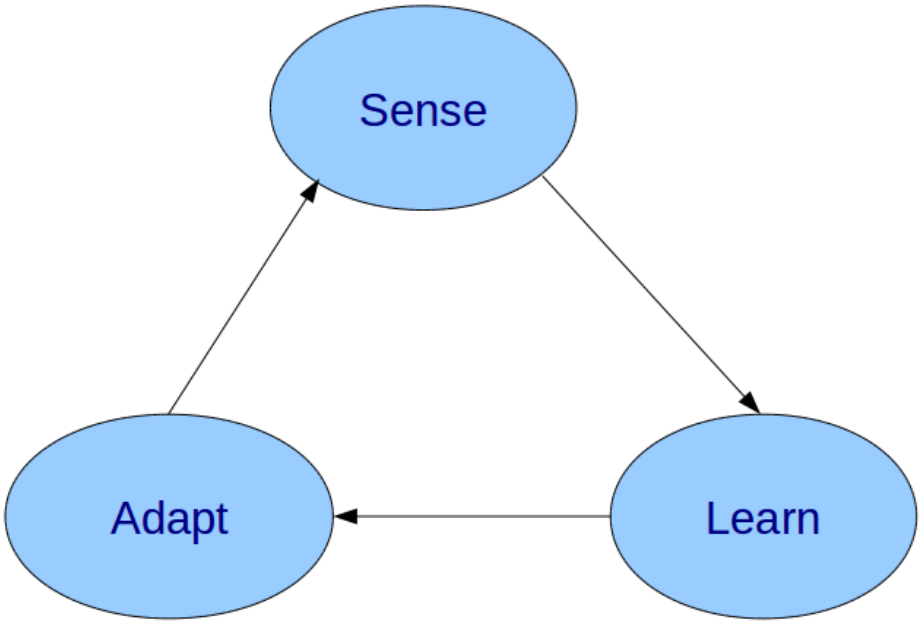

Figure 1.4: Simple Version of Cognition Cycle

Generally, there are three types of cognitive radio. The overlay cognitive radio, shown in Fig. 3.1, utilizes the unused spectrum or spectrum holes to improve

Table 1.1: OFDM via SMSE Analytic Expression

OFMD	Expression
SMSE Analytic	$S_k[m] = \left\{ a_m d_{m,k} e^{-j\left(\theta_{d_{m,k}}\right)} \right\}_{m=0}^{N_f-1}$
Discrete Time Domain	$s_k[n] = \frac{1}{N_f} \mathrm{Re}\left\{ \sum_{m=0}^{N_f-1} (\alpha_{m,k} + j\beta_{m,k}) e^{j(2\pi f_m t_n)} \right\}$

the spectrum utilization efficiency. The underlay cognitive radio, shown in Fig. 1.5(b), transmits ultra-wideband signal with very low transmission power, which is lower than the noise floor, to maintain the co-existence between licensed user and secondary user without harmful interference with each other. In previous works at my research group ([5][6][7][9]), a hybrid overlay/underlay cognitive radio has been proposed, which can improve spectrum efficiency and maximize channel capacity.

1.3 Overview of SMSE Framework

In [10] and [11], a general framework for analyzing, characterizing, and implementing spectrally modulated, spectrally encoded (SMSE) signal was developed. All multi-carrier transmissions, such as OFDM, MC-CDMA, CI/MC-CDMA, and TDCS, are collectively classified as SMSE since data modulation and encoding are applied in the spectral domain, illustrated in Fig. 1.6.

Table 1.1, Table 1.2, and Table 1.3 are popular multi-carrier modulations using SMSE analytic expression, respectively [9].

Table 1.2: MC-CDMA via SMSE Analytic Expression

CDMA	Expression
SMSE Analytic	$S_k[m] = \left\{(\alpha_k + j\beta_k)\, e^{-j(\theta_{c_m})}\right\}_{m=0}^{N_f-1}$
Discrete Time Domain	$s_k[n] = \frac{1}{N_f} \mathrm{Re}\left\{\sum_{m=0}^{N_f-1} (\alpha_k + j\beta_k)\, e^{j(2\pi f_m t_n + \theta_{c_m})}\right\}$

Table 1.3: CI/MC-CDMA via SMSE Analytic Expression

CI/MC-CDMA	Expression
SMSE Analytic	$S_k[m] = \left\{u_m d_k e^{-j\left(\theta_{d_k} + \theta_{o_{m,k}}\right)}\right\}_{m=0}^{N_f-1}$
Discrete Time Domain	$s_k[n] = \frac{1}{N_f} \mathrm{Re}\left\{\sum_{m=0}^{N_f-1} (\alpha_k + j\beta_k)\, e^{j\left(2\pi f_m t_n + \theta_{o_{m,k}}\right)}\right\}$

Table 1.4: TDCS via SMSE Analytic Expression

TDCS	Expression
SMSE Analytic	$S_k[m] = \left\{d_k e^{-j\left(\theta_{d_k} + \theta_{c_m}\right)}\right\}_{m=0}^{N_f-1}$
Discrete Time Domain	$s_k[n] = \frac{1}{N_f} \mathrm{Re}\left\{\sum_{m=0}^{N_f-1} d_k e^{j\left(2\pi f_m t_n + \theta_{c_m} + \theta_{d_k}\right)}\right\}$

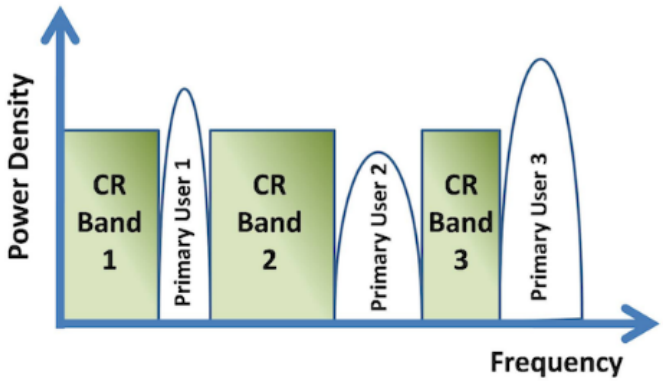

(a) Overlay Cognitive Radio

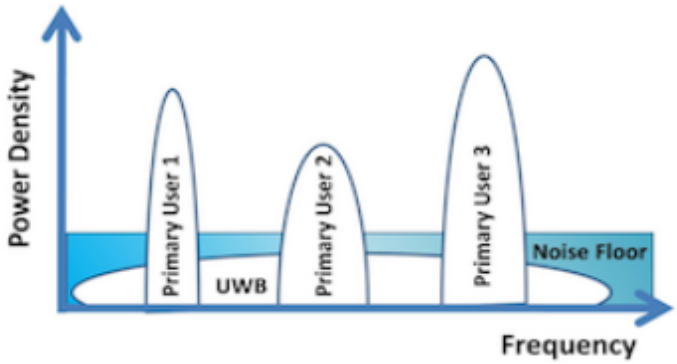

(b) Underlay Cognitive Radio

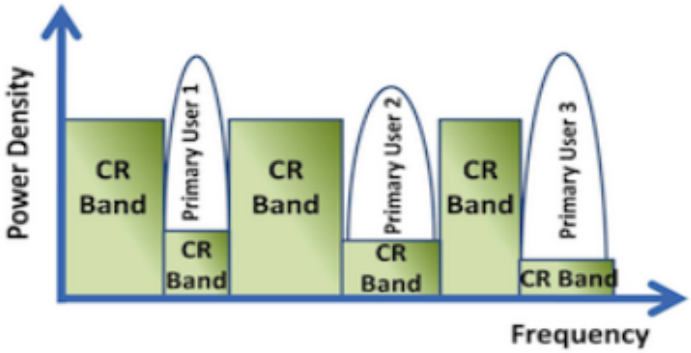

(c) Hybrid Cognitive Radio

Figure 1.5: Coginitive Radios

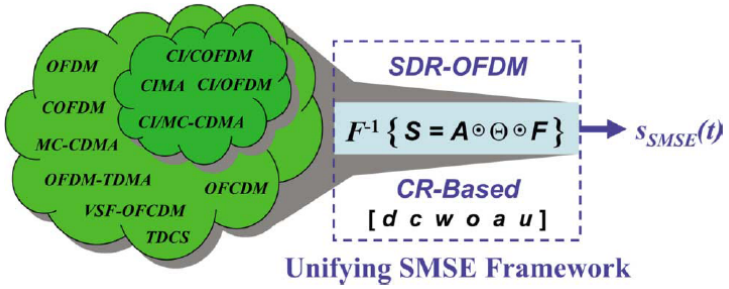

Figure 1.6: Spectrally Modulated Spectrally Encoded Framework

1.4 Overview of Spectrum Sensing

Cognitive radio possesses the ability of adaptivity and awareness, which can make better use of available spectrum [12]. Spectrum sensing is one of the most important tasks in cognitive radios because the spectrum of interest needs to be characterized, meanwhile, the vacant frequency bands should be identified for necessary exploitation. To characterize the spectrum, the cognitive radio devices should be able to identify the vacant spectrum in a fast and efficient way. From the standpoint of the cognitive radios, spectrum sensing has to not only identify spectrum holes, but also aware the operating environment in a multi-dimensional space such as time, frequency, space and code [1].

Different detection and identification of primary users and secondary users schemes have been proposed, such as matched filtering, waveform-based sensing, energy-based sensing, and cyclostationarity-based sensing, in the literature. Matched filtering is known as an optimum detection method if we have a priori knowledge of the primary user signal [13][14][15]. Although it achieves excellent detection performance [16], it requires that the cognitive radio has the perfect knowledge of the primary users' features. On the other hand, it is very complex and impractical on designing the receivers to receive all type of signals. Waveform-based sensing [17][18][19][20] employs known patterns, such as preambles, pilot

tones, and spread sequences, to correlate the received signal [1]. Energy-based sensing detects signal based on received energy [17][21]. The philosophy behind it is computing the energy of the receive signal, comparing it with noise floor, and making the decision to decide if there is a present signal or not. Cyclostationarity-based algorithm detects the primary user by exploiting the cyclostationarity features of the received signals [22][23][24][25].

1.5 Overview of Intercarrer Interference

Multi-carrier transmission such as OFDM has been considered a strong candidate for next generation high-data-rate wireless communication systems [26]. However, multi-carrier transmission is not suitable for mobile communication systems in its original form due to the frequency offset introduced by Doppler shift in high mobility environment. With this frequency offset, the orthogonality among all the subcarriers is lost and inter-carrier interference (ICI) is observed.

Many methods have been proposed in the literature to mitigate the frequency-offset problem to cancel the ICI for OFDM system. Most of such methods use signal processing and/or coding to reduce the sensitivity of the OFDM system to the frequency offset. For example, in [27], authors developed low-complexity minimum mean-square error and decision-feedback equalizer receivers to suppress ICI based on the fact that the ICI power mainly comes from a few neighboring subcarriers. Some researchers also proposed schemes to estimate the frequency offset, including data aided estimation [28][29] and blind estimation [30][31][32]. In the light of the same statement, an effective method known as the ICI self-cancellation scheme has been proposed in [33] where copies of the same data symbol are modulated on L adjacent subcarriers using optimized weights. In [34], a generalized ICI self-cancellation scheme has been proposed. In [35], a ICI self-cancellation using

data-conjugate method is proposed.

1.6 Dissertation Contributions

We have demonstrated an autonomous cognitive radio transmission over multiple non-contiguous spectrum fragments for the first time in the world. This RF demo was invited to be presented at *IEEE DySPAN*, the major conference on cognitive radio and dynamic spectrum access, in April 2010 in Singapore. Our recent demonstration of a cognitive radio in mobile environment received the Best Demo Award at the prestigious *IEEE Globecom* conference in December of 2010.
Specifically, we have:

- Implemented and demonstrated an intelligent spectrum sensing engine via SDR.
- Implemented and demonstrated an overlay cognitive radio which has the ability to stitch all the spectrum holes and operate over non-contiguous multiple bands.
- Implemented and demonstrated the total ICI cancellation to eliminate the ICI without reducing the data rate.
- Implemented and demonstrated the intelligent interference avoidance cognitive radio in static environment and highly mobile environment.

1.7 Dissertation Organization

There are five chapters in this dissertation. Chapter 1 introduces some basic concepts, such as cognitive radio, spectrum sensing algorithms, ICI cancellation schemes,

etc. Chapter 2 introduces the GNU SDR platform, USRP hardware board, and how to build the flow graph using GNU SDR. Chapter 3 discusses implementation and demonstration of an intelligent spectrum sensing engine via SDR to detect the existence of the signals and accurately estimate their RF parameters. Chapter 4 discusses implementation and demonstration of an intelligent interference avoidance SMSE-based cognitive radio. Chapter 5 discusses total ICI cancellation algorithm and its application to the SMSE-based cognitive radio in highly mobile environment.

Overview of GNU Software Defined Radio and USRP

2.1 Overview of Software Defined Radio

Software defined radio (SDR) has been one of the latest and most evolving technologies in the communication industry in civilian, military as well as commercial sectors. SDR is a radio system where the waveform modulation and demodulation are implemented in software domain [4]. Waveforms are generated as sampled digital signals, converted from dignal samples to continous analog signals via a wideband digital to analog converter (DAC) and then upconverterd from intermediate frequency (IF) to radio frequency (RF) via RF front-end. Similarly, the receiver employs a RF front-end to downconvert the RF to IF, feeds the contiguous analog signal to a wideband analog to digital converter (ADC) that captures the raw data of the channels of the SDR. The digitized received signal will be downconverted to baseband which is able to be processed in software. Figure 2.1 shows the concept of an ideal SDR receive and transmit path.

The advantages of using SDR are: (1) SDR offers high flexibility. Developing and debugging software is much easier and low-cost from an operations point of view; (2) SDR could be upgraded easily, which can save both time and cost of the

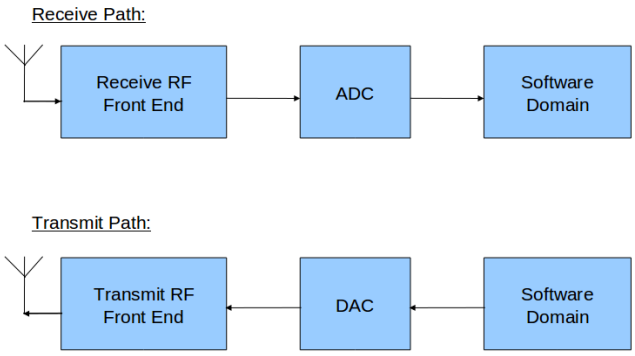

Figure 2.1: Typical Receive/Transmit Path of SDR

design; (3) the software of SDR is reusable; (4) the test of individual signal processing blocks, which are written by the software, the test of performance simulation and the behavioral test are simple and straightforward, so that the same software could be reused for a real, over-the-air system [36]. However, the power consumption of the mobile devices is the weakness of using SDR. Hence, application specific integrated circuit (ASIC), which is customized for a particular use, is necessary for the hardware design to maintain the power consumption as low as possible.

2.2 GNU SDR and USRP

GNU Radio [37] is one of the most popular SDR implementation platform in hobbyist, academic and commercial environments. It is a free software development toolkit which provides the signal processing runtime and processing blocks to implement software radios. Universal software radio peripheral (USRP) is the hardware solution for GNU SDR platform. It enables engineers to rapidly design and implement low-cost, powerful, and flexible software radio systems. USRP connects the software in the host PC and the RF world perfectly via flexible USB2.0 or Giga Byte Ethernet interface.

Figure 2.2 illustrates the receive path of GNU Radio. Receive RF front-end,

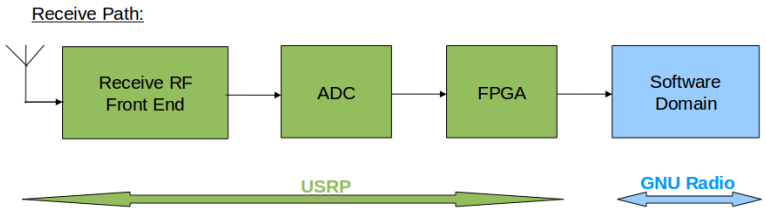

Figure 2.2: Recevie Path of GNU Radio

analog to digital converter, and FPGA are implemented on USRP. GNU Radio provides all signal processing blocks in software domain. The exact inverse is performed in the transmit path. The functionality of each block is explained in detail following.

2.2.1 USRP

The Universal Software Radio Peripheral (USRP) is the hardware solution for GNU Software Radio. The demonstrations in this dissertation use the first generation of USRP. Let's introduce it in detail.

USRP, which integrates microprocessors and digital signal processors on board, has been a low-cost resource for conducting SDR based CR research. The basic design philosophy behind the USRP is that, all the modulation and demodulation waveform specific processings are implemented in software domain; all the high-speed digital up conversion (DUC), digital down conversion (DDC), decimation and implementation are implemented on the FPGA. Figure 2.3 shows a fully populated USRP board. Fig. 2.4 is the diagram of it, from which we could tell that how this hardware module and additional peripherals could perform significant operations.

As the bridge between the continuous analog signal and the discrete digital samples, a USRP motherboard provides up to four 12-bit analog-to-digital converters (ADC) at 64 MS/s, four 14-bit digital-to-analog converters (DAC) at 128

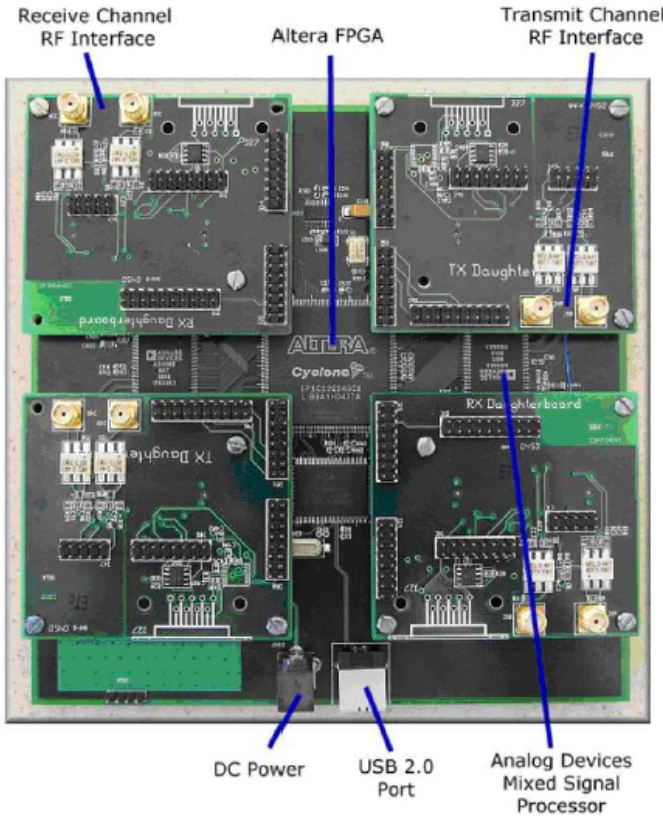

Figure 2.3: Fully Populated USRP Board

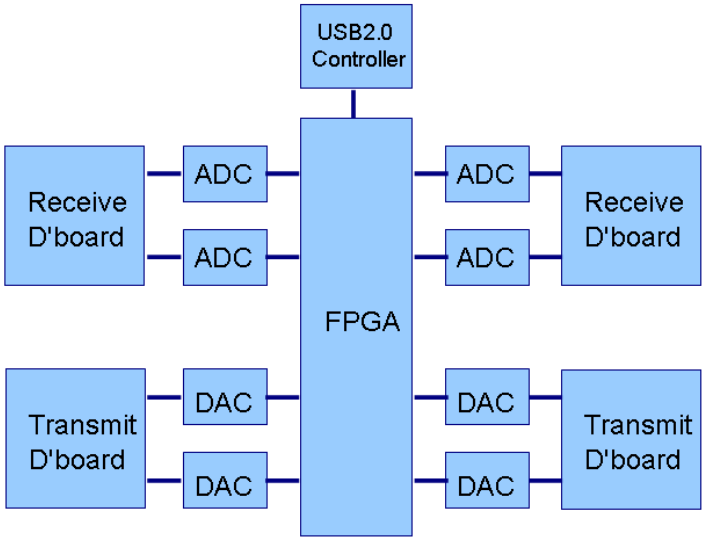

Figure 2.4: Universal Software Radio Peripheral Diagram

Table 2.1: USRP Daughterboards List

D'Board	Type	Operating Range (MHz)
Basic TX/RX	Basic Transmitter/Receiver	1 - 250
LFTX/LFRX	Low Frequency Transmitter/Receiver	DC - 30
TVRX2	Dual TV Band Receiver	50 - 860
DBSRX	Receive-only	800 - 2400
WBX	Wide Band Transceiver	50 - 2200
SBX	Wide Band Transceiver	400 - 4400
XCVR2450	Dual Band Transmitter	2400 - 2500; 4900 - 5900
RFX400	Transceiver	400 - 500
RFX900	Transceiver	750 - 1050
RFX1200	Transceiver	1150 - 1450
RFX1800	Transceiver	1500 - 2100
RFX2400	Transceiver	2300 - 2900

MS/s, a million gate-field programmable gate array (FPGA) and a programmable USB2.0 controller. From Fig. 2.4, we can tell that all ADCs and DACs are connected to the FPGA. The FPGA performs the high-speed general purpose operations, and reduces the data rate feeding to USB2.0. A USB2.0 interface chip is connected with the FPGA. Hence, all of the waveform-specific processings could be performed on the computer via the software.

Each fully populated USRP motherboard can support up to two transmit daughterboards and two receive daughterboards. RF front-end is implemented on the daughterboard. Each daughterboard slot has the access to two of the four high-speed ADCs or DACs. There are a variety of daughterboards that work at different frequency band. By employing a different daughterboard, the designed system can be adapted into a totally different frequency band very easily. Table 2.1 lists all the daughterboards available at this time.

RF Front-End

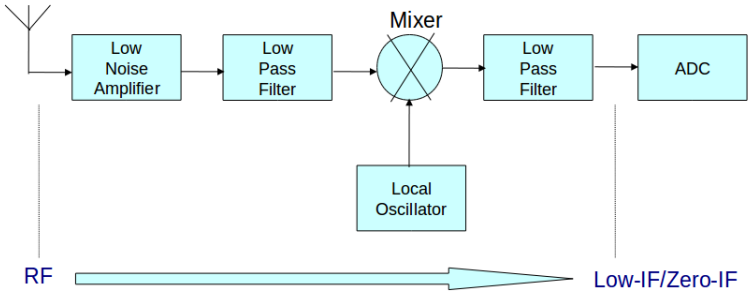

Figure 2.5: The Diagram of RF Front-End of USRP

RF front-end implemented on the USRP daughterboard can convert the RF signal to low-IF [38] or zero-IF [39] with low IF receiver or direct-conversion receiver technology, respectively. The first and second generation TV receive-only daughterboards use low-IF receiver technology, and all other transceivers use zero-IF technology.

Analog to Digital Converter

ADC is the bridge between the continuous analog signals and the discrete digitized samples in the receive path. ADC has two primary characteristics, sampling rate and dynamic range [40]. Sampling rate is the number of times in one second that the ADC measures the analog signal. Dynamic range is the difference between the lowest and highest signal power level that can be distinguished. The quantization level is a function of the number of bits in the ADC. For example, a 12-bit ADC at 64 MS/s on USRP can measure and digitize the analog signal 64 million samples per second with $2^{12} = 4096$ quantization levels.

Field Programmable Gate Array

Altera Cyclone EP1C12 FPGA is integrated on USRP. The FPGA in Figure 2.2 performs high-speed general purpose operations, such as digital-up conversion (DUC), digital-down conversion (DDC), decimation, and interpolation. The USRP is able to sustain 32 MB/s across the USB2.0. Therefore, DDC is employed in receive path to reduce the data rate feeding to USB2.0.

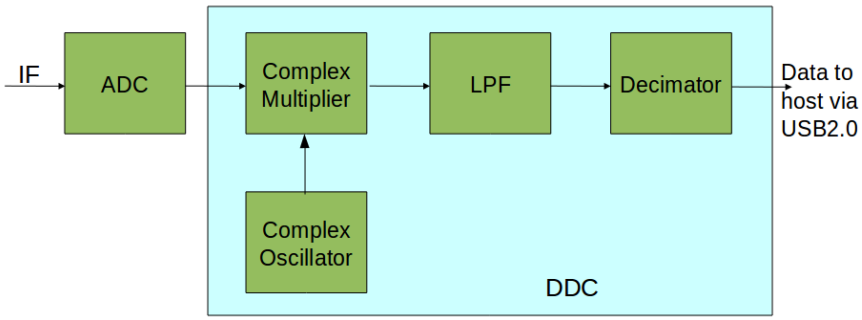

Figure 2.6: The Diagram of DDC on FPGA

Figure 2.6 is the diagram of DDC on FPGA. The DDC can further remove any residual frequency offset caused by the finite tuning steps of the RF front-end on the daughterboard, which is exactly equivalent to the functionality of RF front-end but on digitized samples rather than the analog signal. A decimator is followed to decimate the baseband signal as required for data across USB2.0. DUC is used in the transmit direction. The FPGA of USRP contains multiple instances of DDC and DUC. These instances can be connected to the same or different ADCs to meet the user's need [41].

2.2.2 GNU Radio Design

GNU Radio is an open source Python-based architecture for building SDR projects. It provides software package of signal processing blocks. The user could tie blocks

via Python [42] to create a flow graph. Any block written in C++ provided by GNU Radio Software can be a source with only output ports, such as $usrp.source()$ which is the source of the flow graph through USRP; a sink with just input ports, such as $usrp.sink()$ which is the sink of the flow graph through USRP, or a general block with both input and output ports, such as $gr.multiply\_const\_cc(k)$ which multiplies the input with a constant number k, and outputs the result. We have chosen GNU Radio as the platform and USRP as the hardware solution for our cognitive radio implementation and demonstration.

For any application, from Python's point of view, we just need to select necessary signal source, sink and processing blocks, set proper parameters, and connect all together. In other words, there is nothing but drawing a diagram to show the signal flow from the source to the sink using Python, sometimes with the graphical user interface (GUI) support. A flow graph of SDR may include many sources and sinks and many paths. In a single flow graph, there is no loops, and there must be a connection between each output port and each input port.

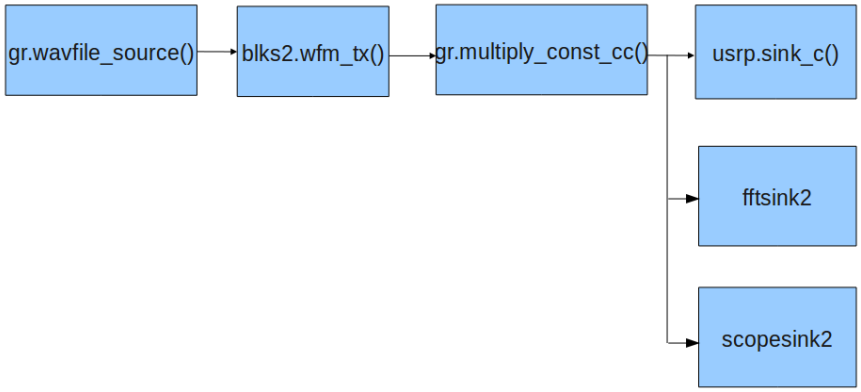

Figure 2.7: GNU Radio Flow Graph

A GNU Radio flow graph of FM-based SDR shows in Figure 2.7. The first block $gr.wavfile\_source()$ generates the source data from .wav file. $blks2.wfm\_tx()$ is the frequency modulator. $gr.multiply\_const\_cc()$ multiplies the input with a con-

```python
#!/usr/bin/env python
from gnuradio import gr, eng_notation, usrp, audio, blks2
from gnuradio.eng_option import eng_option
from optparse import OptionParser
import wx
from gnuradio.wxgui import stdgui2, scopesink2, fftsink2

class fm_tx_path(stdgui2.std_top_block):
    def __init__(self, frame, panel, vbox, argv):
        stdgui2.std_top_block.__init__(self, frame, panel, vbox, argv)

        parser=OptionParser(option_class=eng_option)
        parser.add_option("-f", "--freq", type="eng_float", default=100.1e6,
                          help="set frequency to FREQ", metavar="FREQ")
        parser.add_option("-T", "--tx-subdev-spec", type="subdev", default=None,
                          help="select USRP Tx side A or B (default=A)")
        (options, args) = parser.parse_args()

        self.frame = frame
        self.panel = panel
        self.vbox = vbox
        tone_rate = int(32000)
        self.freq = options.freq
        self.ampl = 200

        # Flow Graph
        self.dac_rate = 128e6  # DAC rate of USRP 128 MS/s
        self.usrp_interp = 400
        self.u = usrp.sink_c (0, self.usrp_interp)
        self.u.set_interp_rate(self.usrp_interp)
        self.usrp_rate = self.dac_rate / self.usrp_interp    # 320 kS/s
        self.sw_interp = 10
        self.audio_rate = self.usrp_rate / self.sw_interp    # sound card rate 32 kS/s

        self.u.set_mux(usrp.determine_tx_mux_value(self.u, options.tx_subdev_spec))
        self.subdev = usrp.selected_subdev(self.u, options.tx_subdev_spec)
        print "Using TX d'board %s" % (self.subdev.side_and_name(),)

        self.subdev.set_enable(True)
        self.subdev.set_gain(self.subdev.gain_range()[1])
        usrp.tune(self.u, 0, self.subdev, self.freq)

        self.src1 = gr.wavfile_source('sky.wav', True) # the source of the flow graph
        self.amplitudes = gr.multiply_const_cc(self.ampl) # the amplifier
        self.fmtx = blks2.wfm_tx(self.audio_rate, self.usrp_rate,max_dev=75e3, tau=75e-6) # FM modulator
        self.time_gui = scopesink2.scope_sink_c(self.panel,title="Time Domain Signal",sample_rate=self.usrp_rate,v_scale=0,
                v_offset=0,t_scale=0,ac_couple=False,xy_mode=False,num_inputs=1,trig_mode=gr.gr_TRIG_MODE_AUTO,
                y_axis_label="Counts",)
        self.vbox.Add(self.gui.win)
        self.freq_gui = fftsink2.fft_sink_c(self.panel,baseband_freq=self.freq,y_per_div=10,y_divs=10,ref_level=50,
                ref_scale=2.0,sample_rate=self.usrp_rate,fft_size=1024,fft_rate=10,average=True,
                avg_alpha=None,title="Frequency Domain Signal",peak_hold=False,)
        self.vbox.Add(self.gui.win)

        self.connect(self.src1, self.fmtx, self.amplitudes, self.u) # connection
        self.connect(self.amplitudes, self.time_gui)
        self.connect(self.amplitudes, self.freq_gui)

if __name__ == '__main__':
        app = stdgui2.stdapp (fm_tx_path, "FM Transmission", nstatus=1)
        app.MainLoop ()
```

Figure 2.8: FM Transmitter in Python

stant number to amplify the signal, the data type of the inputs and the outputs are both complex. There are three sink blocks in the flow graph, $usrp.sink\_c()$ sinks the modulated data onto USRP, converts the baseband signal up to RF analog signal in the air; $fftsink2.fft\_sink\_c()$ and $scopesink2.scope\_sink\_c()$ are graphical user interface which display the frequency domain signal and the time domain signal, respectively. Figure 2.8 illustrates how the flow graph is implemented in Python. It is straightforward to connect the necessary signal processing blocks and show the signal flow from the source to the sinks. One snapshot of time domain and

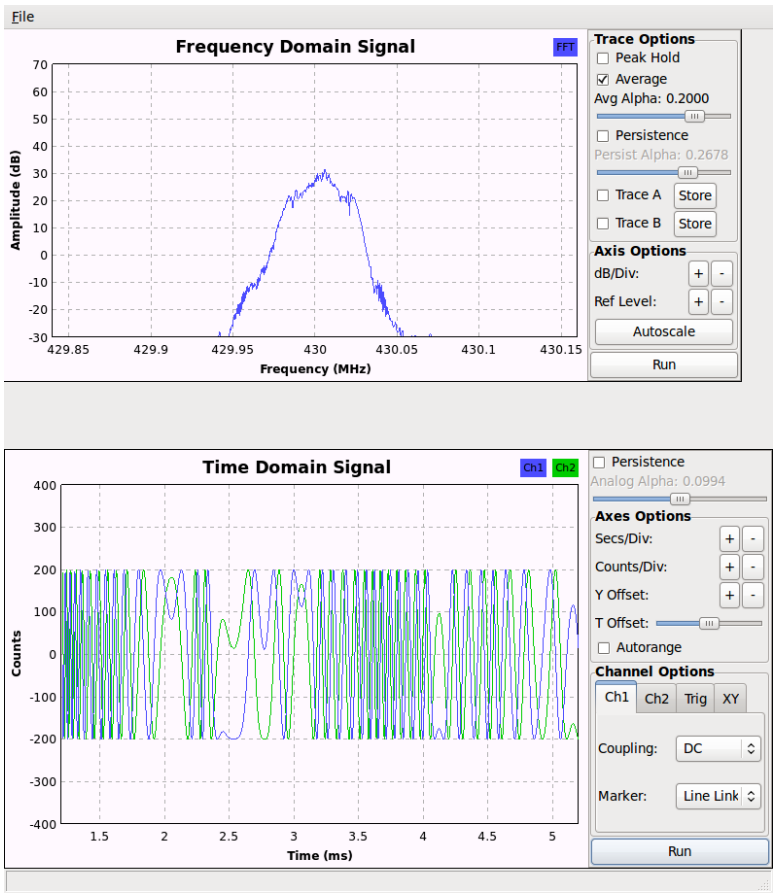

Figure 2.9: Frequency Modulated Signal at the Transmitter

frequency domain FM signal is displayed in Figure 2.9.

2.3 Conclusions

In this chapter, GNU SDR and USRP have been reviewed. An FM-based SDR transmitter has been set up, which can be used as the primary user's trasmission in the following chapters. Throughout the implementations and demonstrations, GNU SDR platform combined with the USRP hardware solution of GNU Radio are used.

SDR-based Spectrum Sensing Engine Design and Implementation

3.1 Introduction

Cognitive radio has the ability to adapt to the dynamically changing environment and make better use of available spectrum [12]. Spectrum sensing is one of the most important tasks in cognitive radio design so that the spectrum of interest can be characterized, meanwhile, the primary user can be detected and its RF parameters, such as center frequency and symbol rate, can be accurately estimated.

Currently, most of existing cognitive radio research is based on the overlay cognitive radio shown in Fig. 3.1. Overlay cognitive radio utilizes the spectrum holes to avoid interference from/to the primary users and coexists with the primary users. Hence, a spectrum sensing is needed to detect the existence of primary user transmission as well as the spectrum holes. Energy based sensing algorithm [18][43][44] is widely used for overlay cognitive radio. Energy based signal detector can identify the vacant spectrum in a fast and efficient way.

However, the spectrum sensing engine needs to provide a spectrum mask for the overlay CR design. Hence, it should have the ability to accurately estimate the important RF paramters so that the CR knows which subcarriers should be

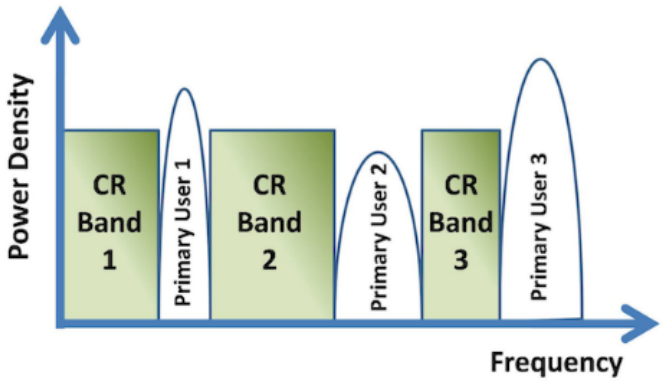

Figure 3.1: Overlay Coginitive Radio

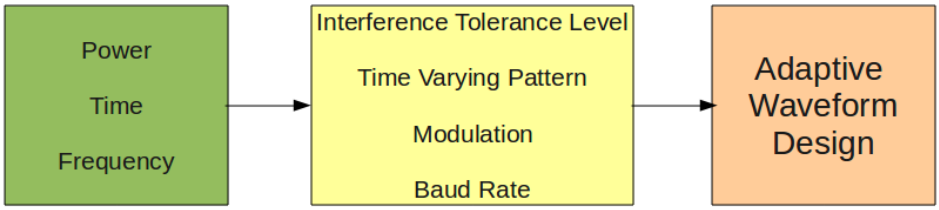

Figure 3.2: Intelligent Spectrum Sensing

turned off to avoid interference to the primary users. Fig. 3.2 illustrates an intelligent spectrum sensing engine. In previous work at our research group, Like has proposed a cyclostationary-based signal detection and classification [45]. I have extended this work and implemented a hierarchical intelligent spectrum sensing engine to estimate important RF parameters of the primary users so that CR can adaptively adjust its transmission waveform to coexist with primary users.

In this chapter, we use USRP and SDR platform [46] to implement and demonstrate an intelligent spectrum sensing engine for cognitive radio network applications. Specifically, we implement a hierarchical cyclostationary-based signal processing algorithm to (1) detect the existence of primary user transmissions; (2) estimate the carrier frequency and symbol rate of the primary user transmission.

3.2 Overview of Spectrum Sensing Algorithm

3.2.1 Overview of Energy-based Detection Concept

Energy detection is a signal detection mechanism using received energy [17][21]. The philosophy behind it is computing the energy of the receive signal, comparing it with noise floor, and making the decision to decide if there is a present signal or not. Energy detection does not need a priori knowledge of the signal.

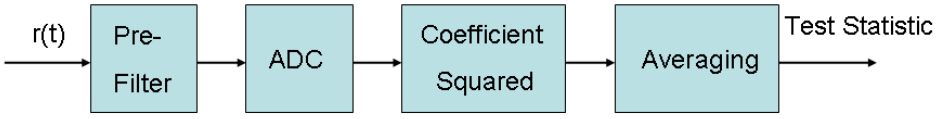

Figure 3.3: Energy-based Detection Algorithm in Time-domain

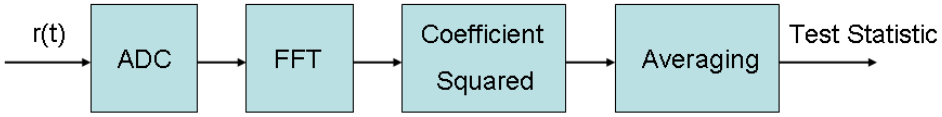

Figure 3.4: Energy-based Detection Algorithm in Frequency-domain

Signal energy can be measured in both time domain and frequency domain. If measuring the signal energy is in a particular frequency region in time domain, a bandpass filter is necessary to match the signal bandwidth, followed by a signal samples energy measurement, which is shown in Figure 3.3, . If the signal energy measurement is in frequency domain, FFT is employed to transform the time domain signal to frequency domain, then the measurement on the combined signal energy over all frequency bins are evaluated, which is shown in Figure 3.4.

Theoretically, either in time domain or in frequency domain, there is no difference in signal detecting and analyzing. Meanwhile, the received signal is

$$r(n) = s(n) + w(n) \tag{3.1}$$

where $s(n)$ is the target signal, $w(n)$ is the white Gaussian noise, n is the sample index for time-domain signal, or FFT symbol index for frequency-domain signal. For simple derivation, the signal sample $s(n)$s are assumed to be independent as a Gaussian random process with zero mean and σ_s^2 variance [17]. The white Gaussian noise sample $w(n)$s are also independent, so the received signal sample $r(n)$s are independent.

Based on the model defined in 3.1, the decision making on the received signal energy is the test of two hypotheses in 3.2. H_0 is the null hypothesis which indicates that the received signal consists of noise only and no signal is present; and H_a, alternate hypothesis, indicates that the received signal composes signal and noise, so the signal is present.

$$\begin{aligned} H_0 &: r(n) = w(n) \\ H_a &: r(n) = s(n) + w(n) \end{aligned} \tag{3.2}$$

As described in [17], the power sensing metric, which is the summation of signal power, is compared to the threshold to make decision:

$$M = \sum_{n=0}^{N-1} |r(n)|^2 \tag{3.3}$$

When there is no signal, the sensing metric is $M = \sum_{n=0}^{N-1} |w(n)|^2$, which should be less than the threshold; when there is a signal present, the sensing metric is $M = \sum_{n=0}^{N-1} |r(n)|^2$, which should be larger than the threshold.

It is well known that under the Neyman-Pearson criteria, the performance of the detection algorithm can be measured by two probabilities: probability of detection P_d and probability of false alarm P_f. A large detection probability P_d is

desired because it is the probability of detecting a signal on a certain frequency band when it is truly present. P_f is the probability of false alarm which happens when the primary signal is present but the detector declares that it is absent. Thus, the smaller the P_f the better. There is a tradeoff between P_d and P_f. Increasing P_d will increase P_f, decreasing P_f will decrease P_d. Hence, we need to find an optimum balance between P_d and P_f. Each pair of P_d and P_f is associated with the particular threshold γ that tests the power sensing metric M. The threshold value is chosen to control the parameters such as P_d and P_f [21][47].

3.2.2 Overview of Cyclic Spectral Analysis for Signal Classification

Modulated signals have built-in periodic features due to the modulated data are coupled with symbol rate, carriers or cyclic prefix, etc. A signal $x(t)$ is considered to be cyclostationary in wide sense if

$$m_x(t + T_0) = m_x(t) \tag{3.4}$$

$$R_x(t + T_0, u + T_0) = R_x(t, u) \tag{3.5}$$

where T_0 is the period of mean m_x and autocorrelation R_x. We can also rewrite (3.5) in Fourier series as [48][49]:

$$\begin{aligned} R_x(t,\tau) &= R_x(t + \tau/2, t - \tau/2) \\ &= E\{x(t + \tau/2)x^*(t - \tau/2)\} \\ &= \sum_{\alpha} R_x^{\alpha}(\tau) e^{j2\pi\alpha t} \end{aligned} \tag{3.6}$$

where α is the cyclic frequency which can be extracted and used as features for identifying transmitted signals [25], and $R_x^\alpha(\tau)$ denotes the cyclic autocorrelation function (CAF), which is given by

$$R_x^\alpha(\tau) = \lim_{T\to\infty} \frac{1}{T} \int_{-T/2}^{T/2} R_x(t,\tau) e^{-j2\pi\alpha t} dt \tag{3.7}$$

when $R_x(t,\tau)$ is periodic in t with period T_0, (3.7) can be expressed as [45]:

$$R_x^\alpha(\tau) = \frac{1}{T_0} \int_{-T_0/2}^{T_0/2} R_x(t,\tau) e^{-j2\pi\alpha t} dt \tag{3.8}$$

The Fourier transform of the CAF is defined as the Spectral Correlation Function (SCF), which is given by:

$$S_x^\alpha(f) = \int_{-\infty}^{\infty} R_x^\alpha(\tau) e^{-j2\pi f\tau} d\tau \tag{3.9}$$

SCF can be measured by the normalized correlation between two spectral components of $x(t)$ at $f + \frac{\alpha}{2}$ and $f - \frac{\alpha}{2}$ over Δt interval. Then, the ideal measurement of SCF can be expressed as:

$$S_X^\alpha(f) = \lim_{T\to\infty} \lim_{\Delta t\to\infty} \frac{1}{\Delta t} \int_{-\Delta t/2}^{\Delta t/2} \frac{1}{T} X_T\left(t, f + \frac{\alpha}{2}\right) X_T^*\left(t, f - \frac{\alpha}{2}\right) dt \tag{3.10}$$

where finite time Fourier transform of $x(t)$ is

$$X_T(t,f) = \int_{t-T/2}^{t+T/2} x(u) e^{j2\pi f u} du \tag{3.11}$$

Fig. 3.5 and Fig. 3.6 illustrate the theoretical SCFs of a BPSK modulated signal and a QPSK modulated signal, respectively. From these two figures, we can observe that (1) for the SCF of BPSK signal, there are four peaks, two appear at

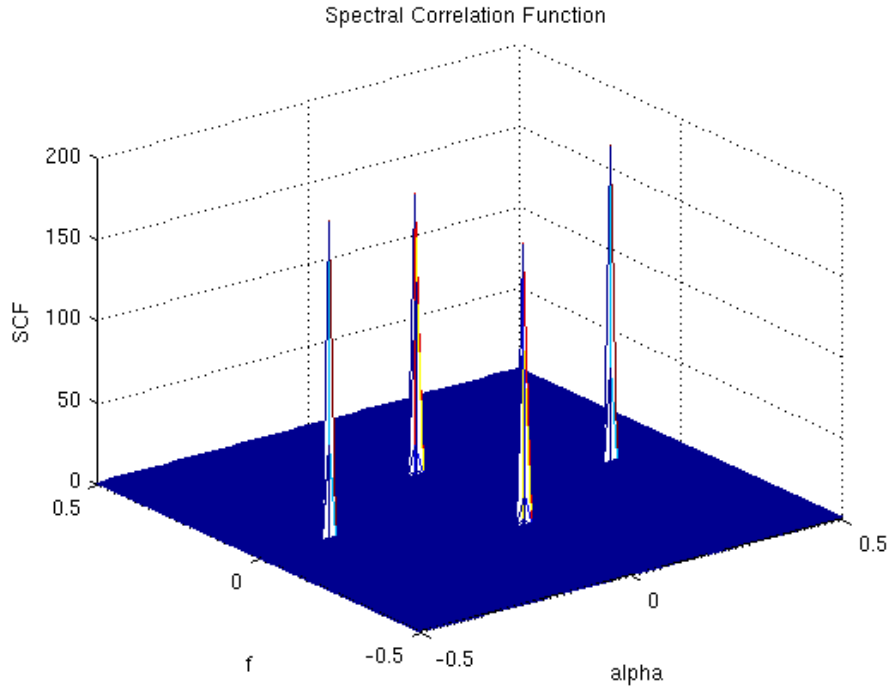

Figure 3.5: The SCF of BPSK Modulation

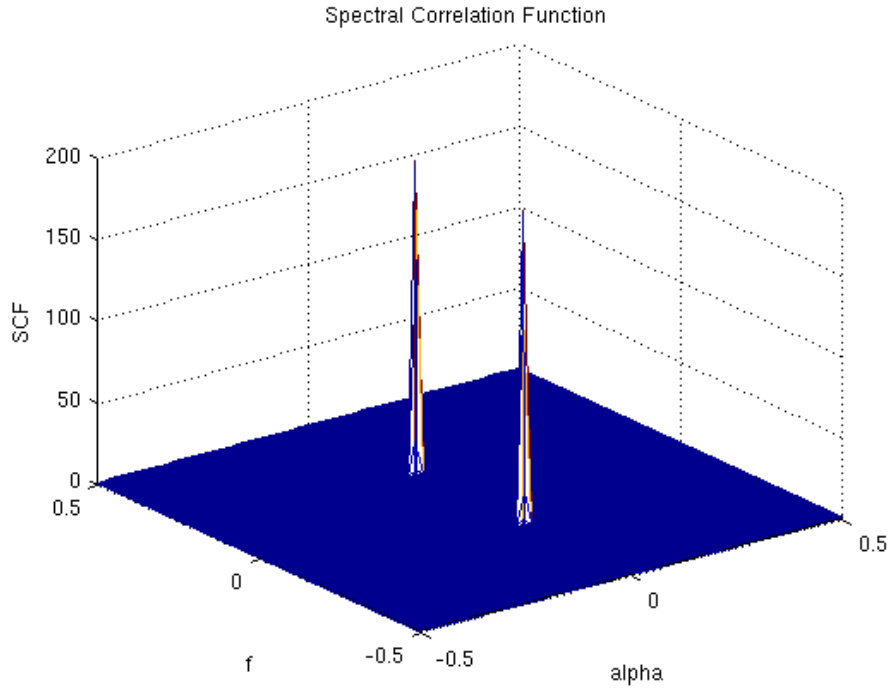

Figure 3.6: The SCF of QPSK Modulaiton

$f = 0$ and $\alpha = 2f_c$, and other two appear at $\alpha = 0$ and $f = f_c$; (2) for the SCF of QPSK signal, there are two peaks at $\alpha = 0$. The two peaks in the cyclic frequency domain at $f = 0$ and $\alpha = 2f_c$ disappear in the SCF of QPSK signal because the in-phase and quadrature components of QPSK signal create cyclic frequency peaks with different sign and cancel each other out. It is obvious that when $\alpha = 0$ the SCF reduces to the power spectrum density (PSD) of the signal. It is important to note that both Fig. 3.5 and Fig. 3.6 are generated from a large number of data. In reality, we can only obtain a short length of RF signal to perform SCF and the in-phase and quadrature components of QPSK signal would not entirely cancel each other's cyclic frequency peaks out. Hence, we will still observe two smaller peaks in cyclic frequency domain.

A significant benefit of using the SCF in spectrum sensing and parameter estimation is its insensitivity to noise. Noise is stationary process, hence the SCF of noise $S_N^\alpha(f)$ is zero when $\alpha \neq 0$. Therefore, SCF provides excellent spectrum sensing and RF parameter estimation in low signal to noise ratio (SNR).

To remove the channel effect, a normalized version of the SCF called the Spectral Coherence Function (SOF) is generated:

$$C_X^\alpha(f) = \frac{S_X^\alpha(f)}{\left[S_X^0\left(f + \frac{\alpha}{2}\right)^* S_X^0\left(f - \frac{\alpha}{2}\right)\right]^{1/2}} \tag{3.12}$$

It can be shown that the channel effects are removed from the SOF and the SOF is preserved as a reliable feature for RF parameter estimation and identification.

In this chapter, we first employ the energy-based algorithm to fast sweep the spectrum, detect the existence of primary users; next, we tune the USRP to the estimated primary user transmission to shrink the data size, employ SCF/SOF to accurately estimate the RF parameters via software defined radio.

3.3 SDR-based Spectrum Sensing Engine Implementation

3.3.1 Energy-based Spectrum Sensing Engine Implementation

An energy-based emission detection is implemented by the software. GNU Radio has built-in signal detection and signal source blocks which, most of the time, can be used directly to facilitate easy signal detection. The signal detection block is an energy based detector that averages the signal over time and estimate the power spectral density (PSD) of the received signal [50]. The layout of the detection pathway is shown in Fig. 3.7.

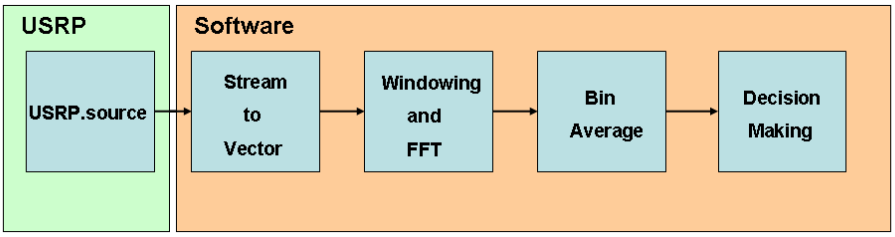

Figure 3.7: The Pathway of GNU Signal Detection

First, the source digitized sample stream is converted into vector with length 256 by stream-to-vector block, then the vector is decimated to a rate for real-time processing. A Blackman-Harris window is applied to every vector with 256 samples. A complex Fast Fourier Transform (FFT) is followed, then averaging block is used to average the magnitudes of each bin over all samples. Last block estimates the PSD.

Fourier analysis assumes that all the real world signal can be approximated as a sum of sinusoids at different frequencies with naturally better approximation when the sum is higher. Fourier analysis is performed using Fourier transform. Since everything is performed in the digital domain, let's see how the Discrete

Fourier Transform (DFT) is defined. The sequence of N complex numbers x_0, x_1, ..., x_{N-1} is transformed into the sequence of N complex numbers X_0, X_1, ..., X_{N-1} by the DFT according to the formula:

$$X_k = \sum_{n=0}^{N-1} x_n e^{-\frac{2\pi i}{N} kn} \tag{3.13}$$

where, $k = 0, 1, \ldots, N-1$, and $e^{\frac{2\pi i}{N}}$ is a primitive Nth root of unity. The phenomenal application of Fourier analysis is the frequency spectrum which is signal harmonic magnitudes plotted versus frequency of the harmonic. This design uses the idea of frequency spectrum as part of the spectrum analysis. The DFT can be computed efficiently in practice using a Fast Fourier Transform (FFT) algorithm. FFT plays a key role in this energy-based spectrum sensing engine.

Since the spectral leakage problem changes the result of the FFT performance significantly, the spectrum analysis is extremely difficult or even impossible. A windowing technique needs to be used to minimize this effect. In this emission detection system, a Blackman-Harris window is applied before the FFT to reduce the side-lobes of the spectrum around the required pulse. The Blackman-Harris window, a straightforward generalization of the Hamming family, is obtained by adding shifted aliased sinc-function. The window is defined for the DFT by

$$\omega(n) = a_0 - a_1 cos(\frac{2\pi}{N} n) + a_2 cos(\frac{2\pi}{N} 2n) - a_3 cos(\frac{2\pi}{N} 3n) \tag{3.14}$$

where $n = 0, 1, 2, \cdots, N-1$ [51]. This Blackman-Harris window is a good window for the small number of terms in their trigonometric series. It minimizes the side-lobes of the spectrum.

On the other hand, due to the USRP hardware limitation, a spectrum which is larger than 8 MHz cannot be examined. To analyze a wide band RF spectrum, for example the 20 MHz FM band or the entire ultra-high frequency (UHF) TV

band, we need to tune the USRP RF front-end in steps so that the wide band is swept over and analyzed. In this section, we will demonstrate the energy-based spectrum sensing engine on FM band and on UHF TV band.

Energy-based Spectrum Sensing Demonstration on FM Band

To examine the 20 MHz FM band from 88 MHz to 108 MHz, we set the decimation rate to 16, which means that 4 MHz spectrum is captured each time. Therefore, the USRP is first tuned to 90 MHz so that 88 MHz to 92 MHz has been covered. After performing complex FFT analysis, the USRP is tuned to the next center frequency 94 MHz to cover 92 MHz up to 96 MHz. We keep tuning the RF center frequency of USRP up to 106 MHz, until the entire 20 MHz FM band frequency spectrum contents have been collected. We make decision on the entire spectrum contents to estimate the RF parameters of the primary FM signals. Fig. 3.8 shows the entire FM band with all the active FM stations as well as the spectrum holes.

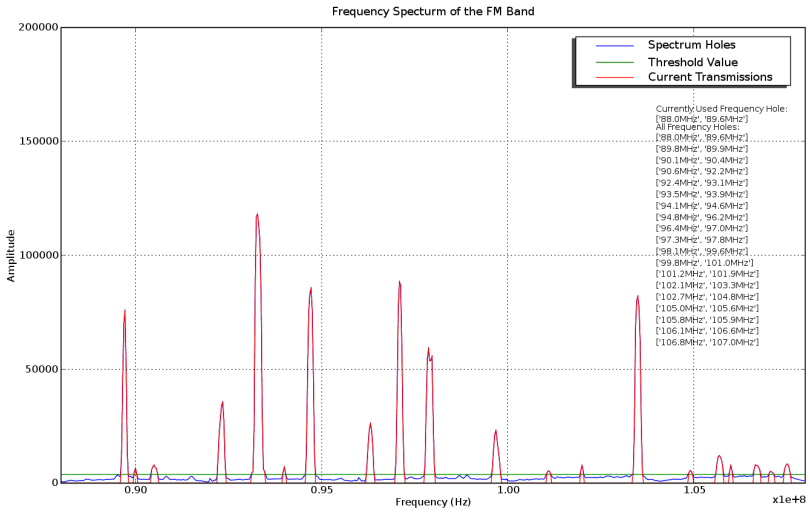

Figure 3.8: Entire FM Band with All the FM Stations and Spectrum Holes

Energy-based Spectrum Sensing Demonstration on UHF TV Band

In this section, we will demonstrate the energy-based spectrum sensing over UHF TV band to detect the active TV stations and the 'white space' over TV spectrum. It is necessary to learn ATSC standard digital TV signal characteristics first. In United States, the digital TV follows the ATSC standard. 8-level vestigial sideband modulation scheme is applied, and the modulated signal uniformly occupies almost the entire 6 MHz TV channel. A pilot tone is located at around 310 kHz above the lower edge of the channel. Fig. 3.9 illustrates that TV Channel 50, which is captured by USRP, occupying 686 MHz to 692 MHz band with a pilot tone about 310 kHz above 686 MHz.

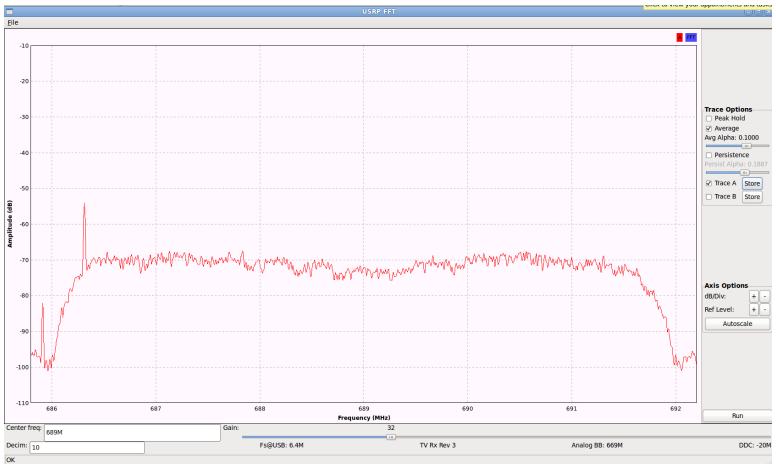

Figure 3.9: TV Channel 50 Captured via TVRX USRP

TVRX USRP daughterboard is employed to sense the whole UHF TV band, which operates from 470 MHz up to 806 MHz. The decimation rate is set to 8 with 25% overlap so that the RF center frequency tune step size is 6 MHz. Fig. 3.10 shows the UHF TV band spectrum sensing result at a given time. TV Channel 26, 30, 41, 50, and 51 are active. There are other transmissions detected at 519.3 MHz, 576.0 MHz, 627.3 MHz, 640.1 MHz, 704.1 MHz, 716.6 MHz, and 768.3 MHz. Meanwhile, according to FCC's Second R&O for White Spaces Order, all the 'white spaces' are determined, 512 MHz to 518 MHz, 524 MHz to 542 MHz, 548 MHz to

566 MHz, 584 MHz to 626 MHz, and 644 MHz to 686 MHz,

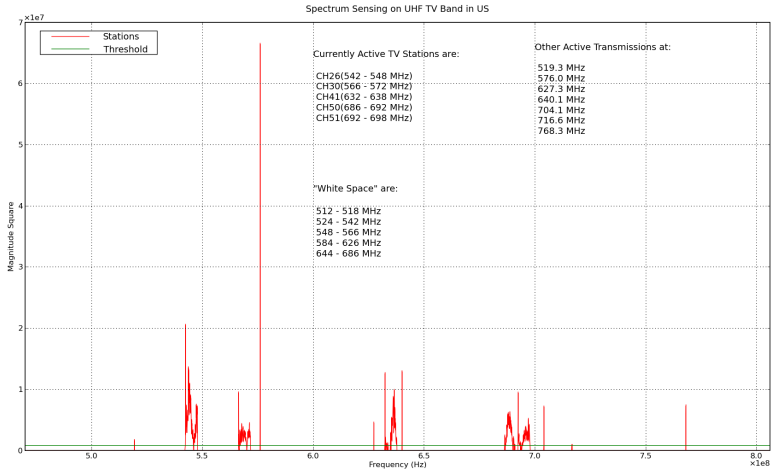

Figure 3.10: Spectrum Sensing on UHF TV Band in US

Other Application - Emission Detector

The energy-based spectrum sensing engine can also be used as an emission detector without knowing the features of the signal. In this demonstration, USRP DB-SRX receive-only daughterboard is used to monitor Cellular Phone Band from 800 MHz up to 2300 MHz in the United States, detects the cellular phone if it is being used, and recognizes the cellular phone by standards, such as GSM850, GSM900, GSM1800, GSM1900, CDMA2000 or W-CDMA.

The designed low-cost wideband emission detector is based on energy detection with bandwidth estimation schemes, thus we need to know some characteristics about cellular phone standards. Global system for mobile communication (GSM) is presently the most successful mobile communication standard worldwide. Channel access is done via FDMA/TDMA and GSM uses FDD/TDD. The modulation mode of GSM is GMSK with a bandwidth time product of BT = 0.3 [52]. GSM consists of GSM850, GSM900, GSM1800 and GSM1900. GSM850 uses 824-849

Table 3.1: Summary of GSM in the US

System	Band	Uplink (MHz)	Downlink (MHz)	BW
GSM850	850	824.0-849.0	869.0-894.0	0.2M
GSM900	900	890.0-915.0	935.0-960.0	0.2M
GSM1800	1800	1710.0-1785.0	1805.0-1880.0	0.2M
GSM1900	1900	1850.0-1910.0	1930.0-1990.0	0.2M

MHz for uplink and 869-894 MHz for downlink, providing 124 RF channels from channel 128 to channel 251. Duplex spacing is 45 MHz. GSM900 uses 890-915 MHz for uplink and 935-960 MHz for downlink, providing 124 RF channels from channel 1 to channel 124 spaced at 200 kHz. Duplex spacing is 45 MHz. In some countries, the GSM900 has been extended, which uses 880-915 MHz for uplink and 925-960 MHz for downlink, adding 50 channels from channel 975 to channel 1023 and channel 0. GSM1800 uses 1710-1785 MHz for uplink and 1805-1880 MHz for downlink, providing 374 channels from channel 512 to channel 885. Duplex spacing is 95 MHz. GSM1900 uses 1850-1910 MHz for uplink and 1930-1990 MHz for the downlink, providing 199 RF channels from channel 512 to channel 810. Duplex spacing is 80 MHz [53].

W-CDMA850 uses 824-849 MHz for uplink providing channel 4132 to channel 4233, and 869-894 MHz for downlink providing channel 4357 to channel 4458. W-CDMA1700 uses 1710-1755 MHz for uplink providing channel 1312 to channel 1513, and 2110-2155 MHz for downlink providing channel 1537 to channel 1738. W-CDMA1900 uses 1850-1910 MHz for uplink providing channel 9262 to channel 9538, and 1930-1990 MHz for downlink providing channel 9662 to channel 9938.

The bandwidth per frequency channel is 0.2 MHz for GSM, 1.25 MHz for CDMA2000, and 5 MHz for W-CDMA. Table I summarizes the features for GSM, and Table II summarizes the features for 3G, which is concentrating on W-CDMA.

Table 3.2: Summary of 3G in the US

System	Band	Uplink (MHz)	Downlink (MHz)	BW
W-CDMA850	850	824.0-849.0	869.0-894.0	5.0M
W-CDMA1700	1700	1710.0-1755.0	2110.0-2155.0	5.0M
W-CDMA1900	1900	1850.0-1910.0	1930.0-1990.0	5.0M
W-CDMA2100	2100	1920.0-1980.0	2110.0-2170.0	5.0M

The emission detector monitors the United State Cellular Phone Band from 800MHz up to 2300MHz, detects the cellular phone if it is being used, and recognizes the cellular phone by standards via different operating frequency. The emission detector scans the entire spectrum from 800MHz to 2300MHz every 2 seconds, displays and reports any emission in the real-time. Fig.3.11, one of the snapshot, shows that the system is sensing spectral environment, and detecting a GSM850 cellular phone at 844MHz. Fig.3.12, another snapshot, indicates that the system detects that two cellular phones are being used, and recognizes them by their standards, a GSM850 detected at 848MHz and GSM1900 detected at 1873MHz. The designed detector can detect multiple emissions simultaneously as long as they are within this band.

3.3.2 Cyclostationary-based Spectrum Sensing Engine Implementation

In section 3.3.1, the energy-based spectrum sensing engine has been demonstrated and implemented to detect the existence of primary users. Based on the sensing result, we will fine tune the USRP around to the emission's center frequency to reduce the collected data size. For example, a RFX400 USRP daughterboard is used to sweep the spectrum from 400MHz to 450MHz. If there is an emission detected

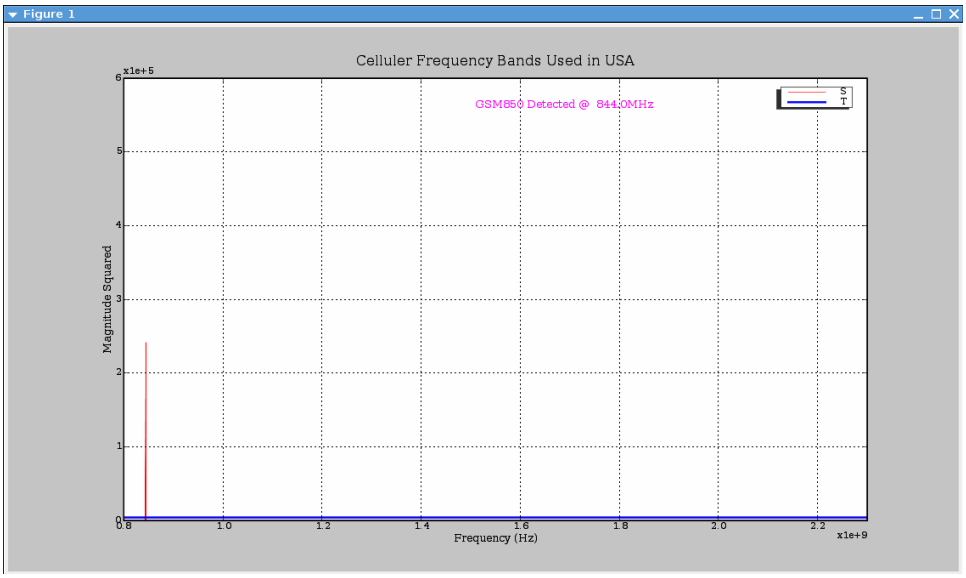

Figure 3.11: GSM850 Detected at 844MHz

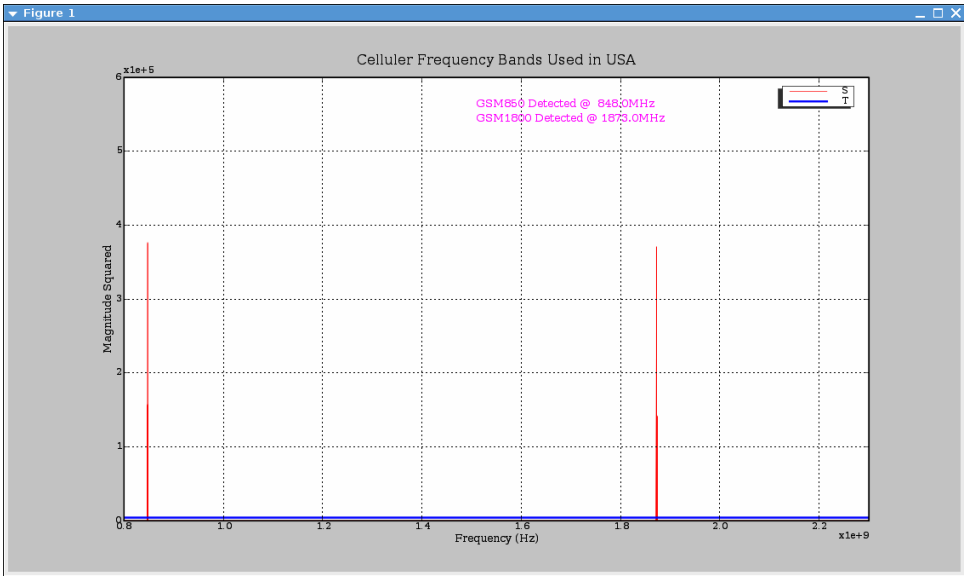

Figure 3.12: GSM850 at 848MHz and GSM1900 at 1873MHz

through energy-based detector around at 430MHz with about 100kHz bandwidth, we will tune the USRP RFX400 to 430MHz with 256 decimation rate. Hence, the reduced size data are collected and RF parameters can be accurately estimated by cyclostationary-based algorithm.

In this section, we use Tektronix arbitrary waveform generator (AWG) to generate the primary user's signal. Next, the signal is fed into a Spirent SR5500 wire-

less channel emulator to emulate the channel effect such as multi-path, Doppler shift, and additive Gaussian noise. Finally, a USRP SDR receives the primary user's signal, down-convert it to baseband. The intelligent spectrum sensing engine residing on the software defined radio performs (1) primary user detection; (2) RF parameter estimation. Fig. 3.13 illustrates the system setup.

Figure 3.13: System Setup for Intelligent Spectrum Sensing

Tektronix Arbitrary Waveform Generator

Tektronix arbitrary waveform generator (AWG7062B) with 6 GS/s can easily generate very complex signals complete with controllable jitter, noise and other signal impairments [54]. In this demonstration, we use AWG7062B to generate different kinds of primary user's signals.

Spirent Wireless Channel Emulator

The SR5500 Wireless Channel Emulator (WCE) [55] is a complete and efficient channel emulator that provides various built-in multi-path fading channel model, Doppler shift and additive white Gaussian noise functions. We use Spirent SR5500 to mimic the multi-path fading channel of the transmitted primary user signals.

Intelligent Spectrum Sensing Demonstration

We first apply an energy based spectrum sensing algorithm to sweep 10 MHz bandwidth to roughly estimate the primary user's carrier frequency and band-

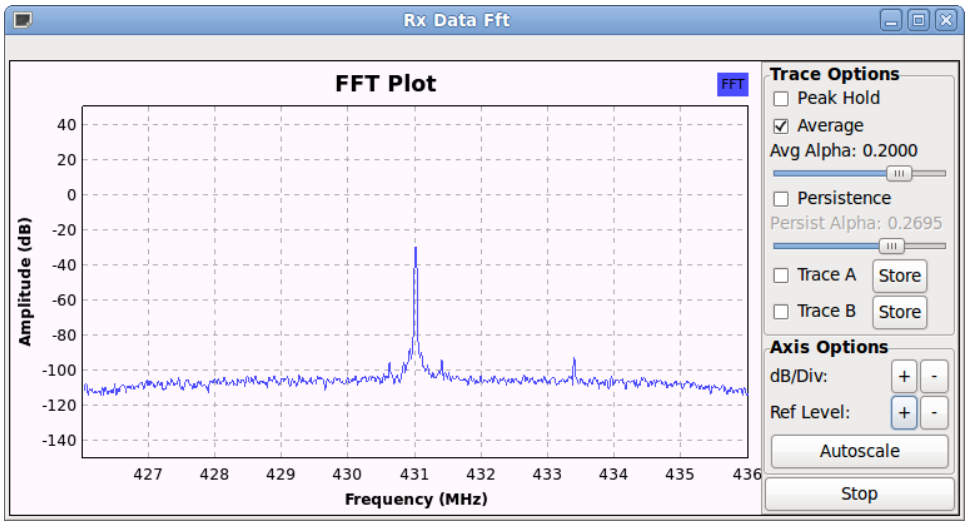

Figure 3.14: Sweeping the Spectrum with 10MHz Bandwidth

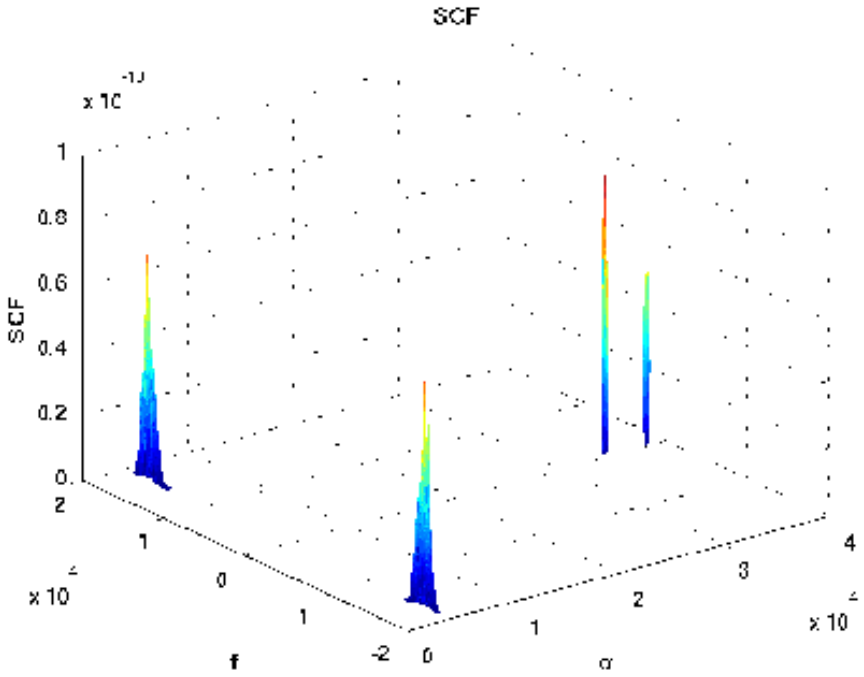

Figure 3.15: SCF of the Signal Received via USRP

width. Fig. 3.14 shows an example of the sweeping result. Here, it can be seen that a primary user's signal exists somewhere between 430.5MHz to 431.5MHz with bandwidth about 5 kHz. This coarse estimated carrier frequency and symbol rate are fed into the SCF and SOF generator to perform a high-resolution RF parameter

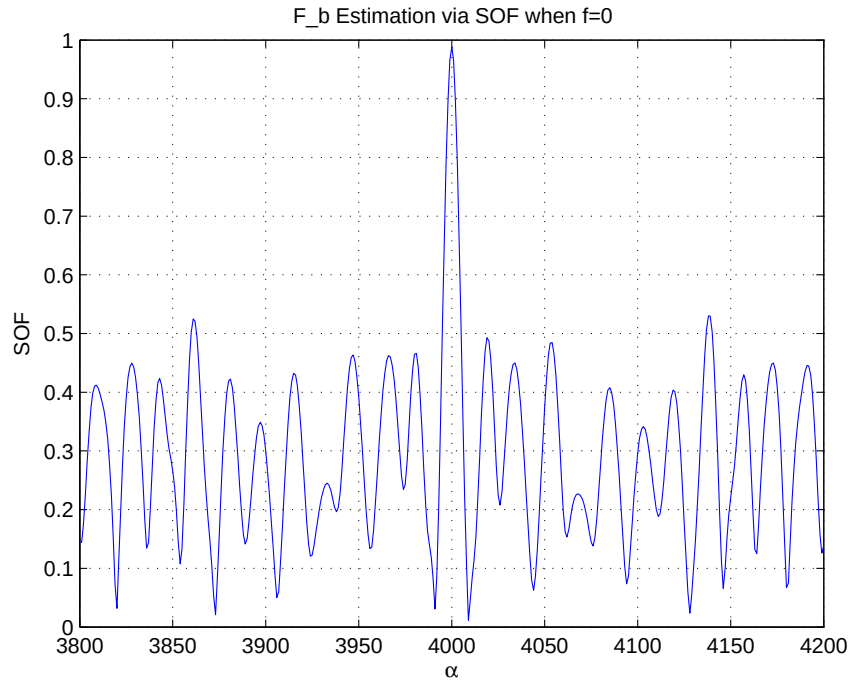

Figure 3.16: Data Rate

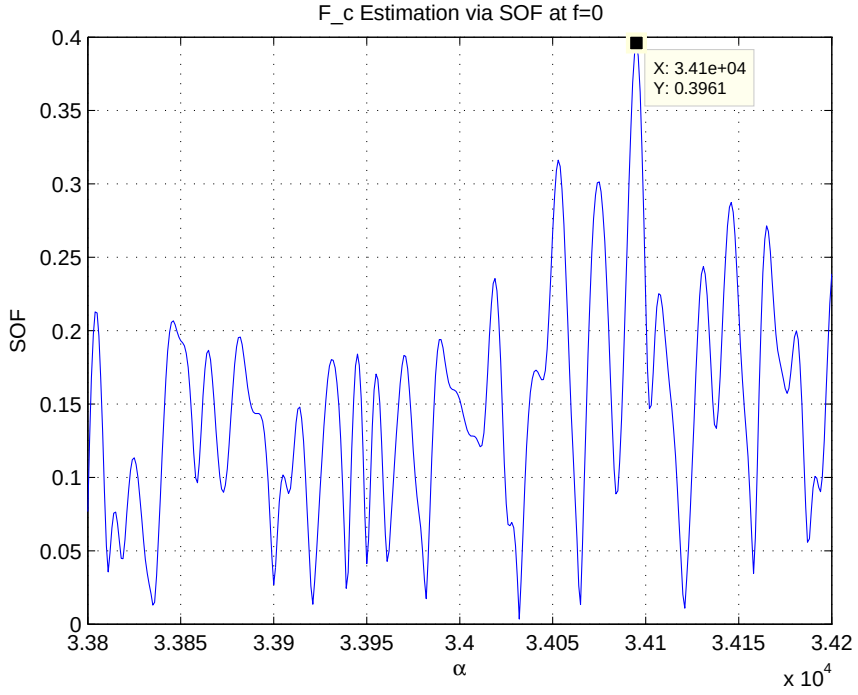

Figure 3.17: Estimation of Center Frequency f_c

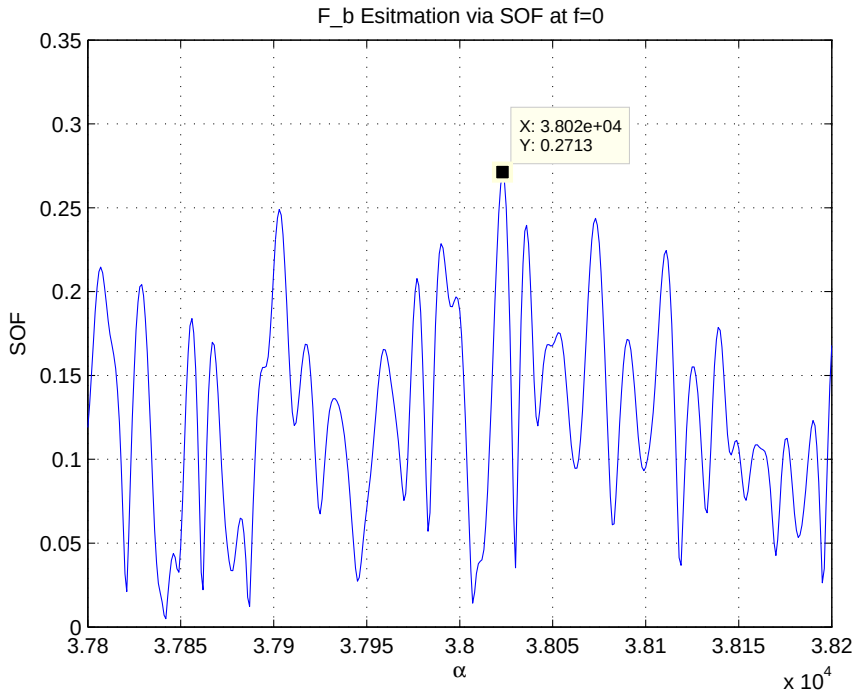

Figure 3.18: Estimation of Bit Rate F_b

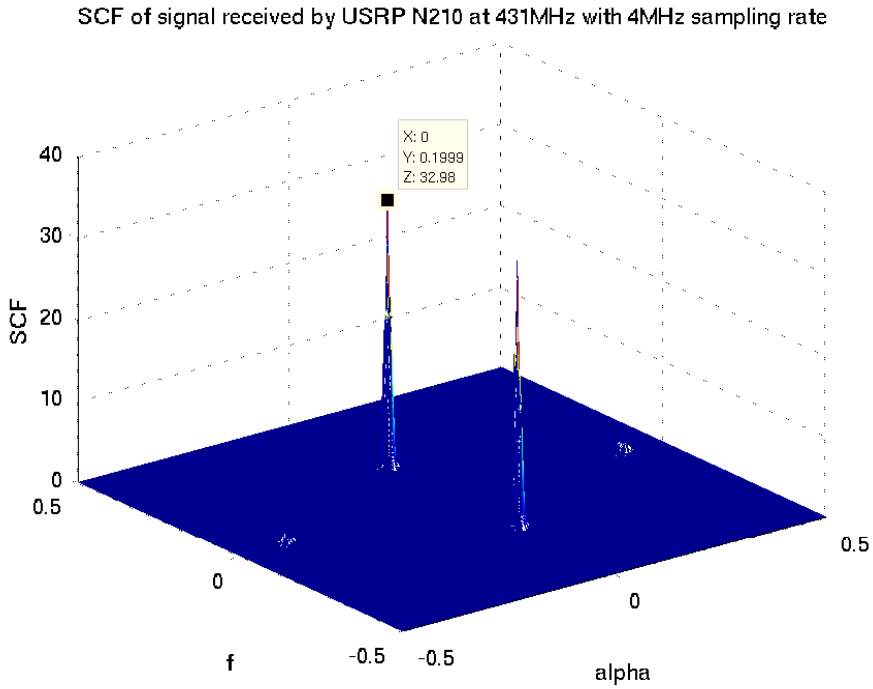

Figure 3.19: SCF of QPSK Signal Received by USRP

estimation.

In example 1, we use the Tektronix AWG to generate a BPSK signal at 431.017 MHz and feed the signal to Spirent WCE. The WCE introduces multi-path, adds noise and provides a Doppler shift to the signal. Then, we use USRP to collect the signal at 431 MHz with 80k sampling rate. Fig. 3.15 illustrates the SCF obtained by the intelligent spectrum sensing engine. By observing the SCF of the received signal, we can easily determine its modulation type is BPSK since there is a peak in cyclic frequency domain with similar height to the peaks observed in the frequency domain.

Next, by calculating high resolution SOF around coarsely estimated symbol rate and carrier frequency, we obtain very accurate estimation of both parameters. Fig. 3.16 to Fig. 3.18 show the detailed SOF of the signal in cyclic frequency domain ($f = 0$). In Fig. 3.16, a spectral line is observed at $\alpha = 4000Hz$, which is the estimated symbol rate of the signal. In Fig. 3.17, a spectral line is observed at $\alpha = 2f_c = 34100$. The estimated baseband center frequency can then be calculated as $17050Hz$. Adding the 431 MHz down-convertion frequency back, the estimated transmitted signal center frequency is then 431.01705 MHz. The frequency offset between estimated carrier frequency and transmitted frequency is due to the Doppler shift introduced by the channel. Therefore, an accurate center frequency is estimated.

In example 2, we use AWG to generate a QPSK modulated signal at 431.017 MHz and use USRP to receive the signal at 431 MHz. Fig. 3.19 shows the SCF plot of the received signal. Compared to the SCF of BPSK, it is obvious that this is a QPSK modulated signal since the cyclic frequency peaks have much lower height. However, by zooming in the cyclic frequency projection of SOF, symbol rate f_b and carrier frequency f_c can be estimated as shown in Fig. 3.20 and Fig. 3.21.

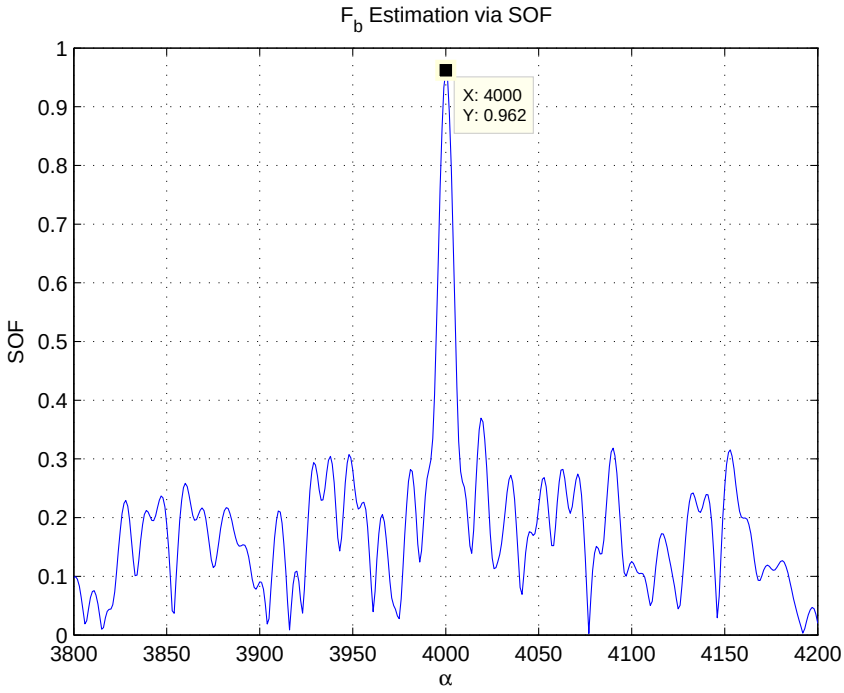

Figure 3.20: Estimation of Bit Rate F_b, QPSK

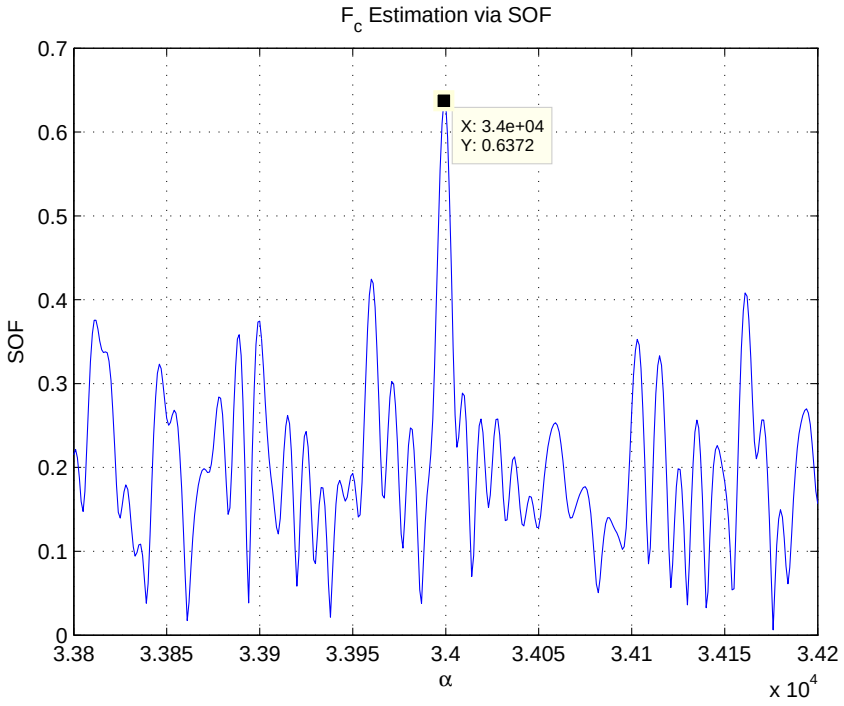

Figure 3.21: Estimation of Bit Rate F_c, QPSK

3.4 Conclusion

In this chapter, we have implemented and demonstrated an intelligent spectrum sensing engine for cognitive radio network using GNU Radio with USRP SDR platform. We first use energy-base detection algorithm to sweep the wide band quickly and detect the existence of signals. Then, we fine tune the USRP to the band of interest to shrink the data size and employ the second-order cyclic features SCF and SOF to accurately estimate the carrier frequency and symbol rate of the primary user's signal. Without any a priori knowledge of the primary user, the intelligent spectrum sensing engine blindly estimates the center frequency and baud rate very accurately.

SMSE-base Overlay Cognitive Radio Implementation and Demonstration

4.1 Motivation

With the emergence of increasing number of wireless devices, the radio spectrum becomes scarce. Recent studies indicate that most of the time wide ranges of the radio spectrum are rarely utilized while other bands are heavily utilized. Hence, the scarcity is mainly due to the inefficient spectrum usage. Cognitive radio arises to be a possible solution to spectral crowding problem by introducing the opportunistic usage of frequency bands that are not heavily occupied by licensed users [56]. As an intelligent wireless system, it has the capability of sensing the spectrum, being aware of its surrounding environment, dynamically adjusting the radio operating parameters, and autonomously adapting itself into the environment to meet user needs.

Specifically, to achieve this goal, the PHY (physical layer) of CR needs to be highly flexible and adaptable [1]. Multi-carrier technology is the most widely used technology for CR, such as OFDM (orthogonal frequency division multiplexing), MC-CDMA (multi-carrier code division multiple access), CI/MC-CDMA (carrier interferometry/multi-carrier code division multiple access), and TDCS (transform-

domain communication system) [57]. The beauty of using multi-carrier technology is that the subcarriers can be easily turned on and off. The secondary user can generate a wide band multi-carrier waveform. If there is a primary user active within the band, the secondary cognitive radio just needs to turn off the subcarriers which are occupied by the primary user to provide the coexistence between the primary user and the secondary cognitive radio. This is called overlay cognitive radio.

In this chapter, we present an adaptive interference avoidance cognitive radio implementation using USRP software defined radio boards and GNU radio software platform. Specifically, we employ SMSE framework to generate multi-carrier waveform for secondary cognitive radio. Combined with a spectrum sensing engine, the cognitive radio detects the availability of each and every subcarrier in the operational bandwidth. By turning off those subcarriers occupied by the primary users, the cognitive radio implements a non-contiguous multi-carrier transmission. There are a few unique features of our cognitive radio implementation: (1) we have demonstrated real time seamless video transmission without interference to primary users and from primary users; (2) our cognitive radio is capable of taking advantage of multiple spectrum holes and operating over multiple non-contiguous spectrum bands; (3) the cognitive radio dynamically adjusts which subcarriers to turn off according to the primary users' transmission; (4) the cognitive radio can also easily adjust other parameters such as the total number of subcarriers, center frequency, and bandwidth of each subcarrier.

4.2 Design Solution

Overlay CR is designed using SMSE framework to generate multi-carrier waveform which can autonomously avoid interference to and from the existing users.

Fig. 4.1 shows the overlay CR implementation setup. Two SDR-based CR nodes are in the system. PU_TX and PU_RX are primary user's transmitter and receiver, respectively. SU_TX and SU_RX are cognitive radio's transmitter and receiver, respectively. The primary user in the system could transmit either a narrow band FM transmission with about 200kHz bandwidth or a wide band digital modulated transmission with 2MHz bandwidth.

The designed secondary user's bandwidth is 2MHz. To demonstrate the functionality of the overlay CR, we build a transmission between PU_TX and PU_RX with (1) narrow band transmission so that CR can turn off the subcarriers and transmit over non-contiguous multi-carrier band; (2) wide band transmission, which means the primary user will operate on the entire 2MHz bandwidth, so that the CR could perform the spectrum mobility feature. FM and GMSK modulation are employed by PU. Multi-carrier waveform with 64 subcarrier is applied for SU. USRP RFX400 and RFX2400 daughterboards are used to perform that it is easy to demonstrate the intelligent interference avoidance SMSE-based cognitive radio node on different band by using different USRP daughterboards.

The SDR-based spectrum sensing engine on SU_TX will first sense the spectrum, detect the primary user and classify the signal by narrow/wide band. If no primary users are active within 2MHz band, the SU will transmit a contiguous multi-carrier waveform carrying seamless real-time video signal. If a PU is detected, SU will first analyze the spectrum and classify the signal by narrow band or wide band transmission. If the bandwidth of PU is narrow, a non-contiguous multi-carrier waveform can be applied by turning off the subcarriers occupied by the PU, thus the CR operates over non-contiguous multi-band to avoid interference from and to the PU. If the bandwidth of detected signal is 2MHz, there is no spectrum available for CR. Hence, the spectrum mobility feature is performed. SDR-based spectrum sensing engine should allocate a new spectrum holes to SU,

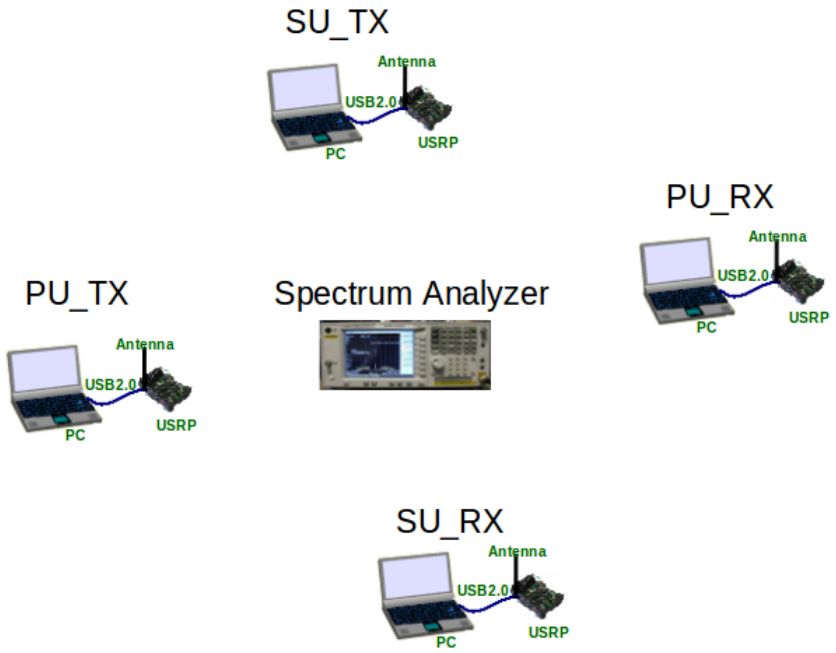

Figure 4.1: Overlay Cognitive Radio Implementation Setup

where it can use contiguous or non-contiguous multi-carrier technology. The spectrum analyzer in the system will validate all the unique features of the intelligent interference avoidance SMSE-based CR node.

4.3 Spectrum Sensing and Adaptation

With the aid of spectrum sensing engine, PU is detected, important RF parameters are estimated, and a spectrum mask is provided for the SMSE-based multi-carrier waveform generator.

If no PU is detected, SU_TX adapts to the environment and transmit a contiguous multi-carrier waveform to SU_RX. If one PU is detected, the learning and adaptation process which resides on SU_TX estimates the center frequency of PU, meanwhile, classifies the signal by the signal bandwidth. If a narrow band PU transmission is determined, the adaptation process calculates which subcarriers are interfering to PU and turn these subcarriers off. A control signal is send to the

SU_RX to indicate the subcarriers that are off. Meanwhile, an overlay multi-carrier waveform is generated by the software. If a wide band PU transmission is determined, the spectrum sensing engine will search for other available spectrum holes which can accommodate 2MHz transmission. Again, the control signal will inform the SU_RX to switch to the new center frequency.

Throughout the demonstration, we assume the control signal does not interfere from/to the primary users. We have a fix band for the control signal.

4.4 SMSE-based Overlay CR Implementation via SDR

To implement and demonstrate the overlay CR via GNU SDR, we employ SMSE framework to generate multi-carrier waveforms. Specifically, as shown in Fig. 4.2, if the entire 2MHz band could be used by the CR, a contiguous multi-carrier waveform is generated. If a narrow band primary user is active within the 2MHz band, some of the subcarriers which are occupied by the primary user need to be turned off, which is in dot line shown in Fig. 4.2. Hence, a non-contiguous multi-carrier waveform is generated.

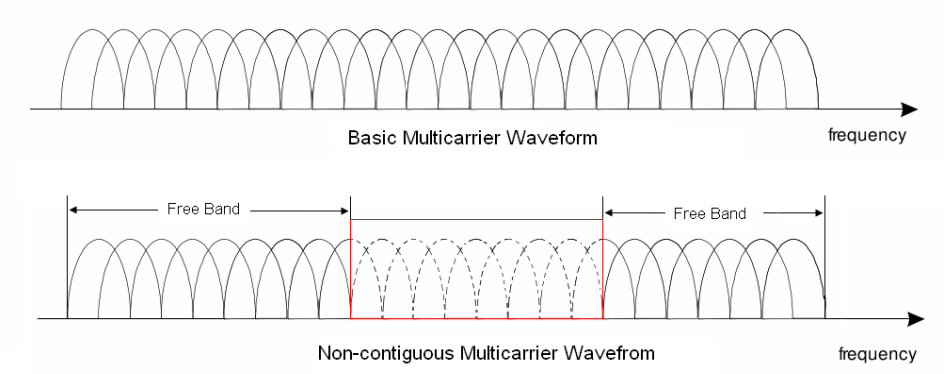

Figure 4.2: Contiguous Multi-carrier Waveform vs. Non-contiguous Multi-carrier Waveform

The block diagram of the SMSE encoder and decoder is illustrated in Fig.

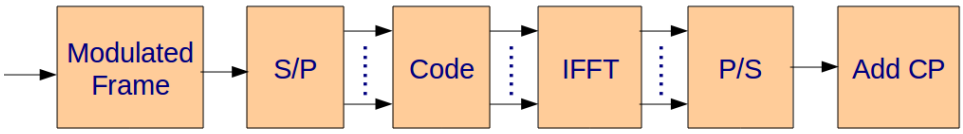

(a) Transmit Path

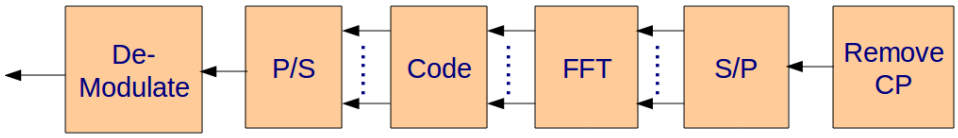

(b) Receive Path

Figure 4.3: SMSE Encoder/Decoder Block Diagram

4.3(a) and Fig. 4.3(b), respectively. The modulated frame truncates the modulated data to the frames with inserted preambles for frame detection and synchronization [58]. The serial data are converted to parallel which is fed to the code block, followed by the IFFT block to get the time domain symbols. Cyclic prefix (CP) is added to avoid inter-symbol interference (ISI). In the receive path, after removing the CP, the serial symbols are converted to parallel which passes through the FFT block to obtain the frequency domain symbols. Then, the symbols multiply the transpose conjugate of the code to get the data which can be demodulated after the parallel to serial block.

The overview of SMSE-based cognitve radio block diagram is shown in Fig. 4.4. The webcamera with microphone captures the real-time video and audio signals. Video and audio codec is implemented by VideoLAN, which is a complete software solution for media streaming developed under the GNU General Public License. The video and audio streaming is fed into the SMSE-based multi-carrier waveform generator. The intelligent spectrum sensing engine senses and learns the environment, and provides the spectrum mask to the SMSE encoder. There-

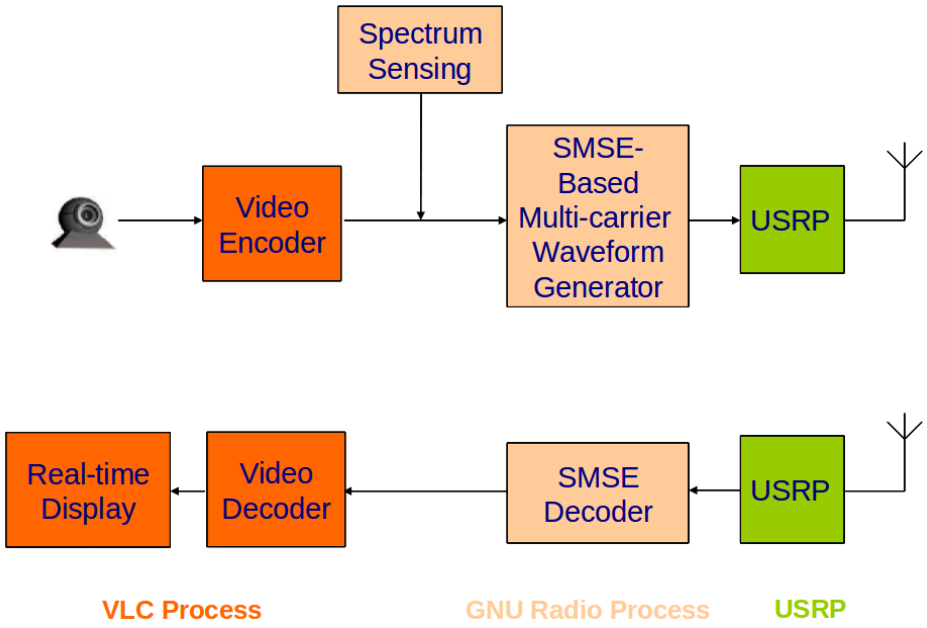

Figure 4.4: SMSE-based Cognitive Radio Block Diagram

fore, the contiguous or non-contiguous multi-carrier waveforms could be generated. Last, the data are fed into the USRP via USB2.0 to convert the digitized samples to analog signal, and upconvert the baseband signal to RF signal. The receive path is vise versa. After the USRP downconverts the RF to baseband and converts to digital signal, the SMSE decoder is applied to demodulate the data, which is sent to the VideoLAN to decode the video/audio signal and real-time play it.

The spectrum sensing engine resides on the SU_TX. To reduce the size of collected data for sensing, packets-based sensing strategy is used. Specifically, the SU_TX senses the spectrum, learns the environment, adapts itself to the dynamically changed environment, sends the control signal to SU_RX, and transmits real-time video. After every 200 packages are sent, the SU_TX transmission halts and the spectrum sensing performs, followed by the transmission. The circle does not stop until the user terminates it. The transmitter state diagram shown in Fig. 4.5 illustrates how this SU_TX works.

At the receiver side, SU_RX listens to the control signal, which includes center

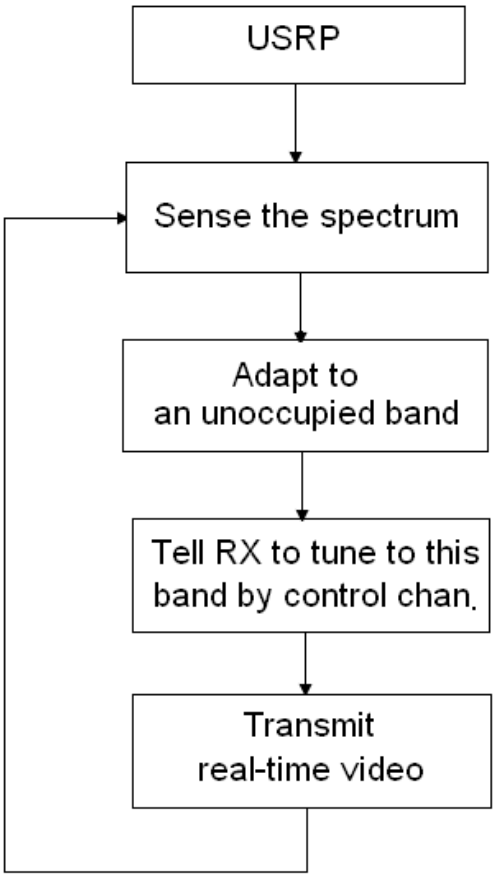

Figure 4.5: Transmitter State Diagram

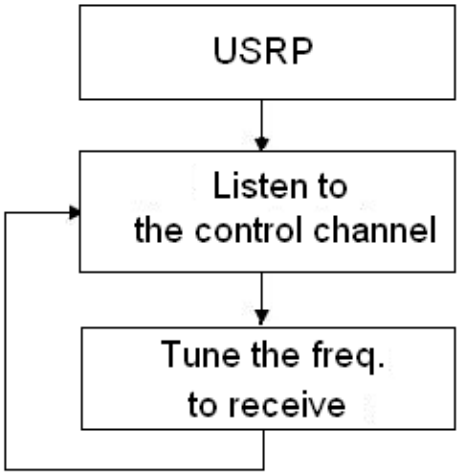

Figure 4.6: Receiver State Diagram

frequency, total number of subcarriers, which subcarriers are tuned off, etc. Then, it adjusts the parameters according to the control signal and receives the data. After receiving 200 packets, it goes back to listen to the control signal. Meanwhile, the video streaming is played in real-time. Fig. 4.6 illustrates how SU_RX works.

Fig. 4.7 shows the spectrum captured by the USRP board when the cognitive radio is operating over one contiguous spectrum hole. Evidently, if no narrow band transmission exists in the transmission band, the designed CR transmits over the entire 2MHz band. Fig. 4.8 shows the non-contiguous multi-carrier spectrum. It is obvious from this figure that the cognitive radio operates over two non-contiguous bands by transmitting a non-contiguous multi-carrier waveform by turning off a few subcarriers around the frequency of 430.5MHz of the primary user. Fig. 4.9 shows when the primary user jumps to a different frequency, 431.5MHz, the cognitive radio dynamically changes the waveform by turning off some other subcarriers to avoid interference dynamically. As a direct result, the real time video and audio transmission supported by the cognitive radio link experiences no interruption.

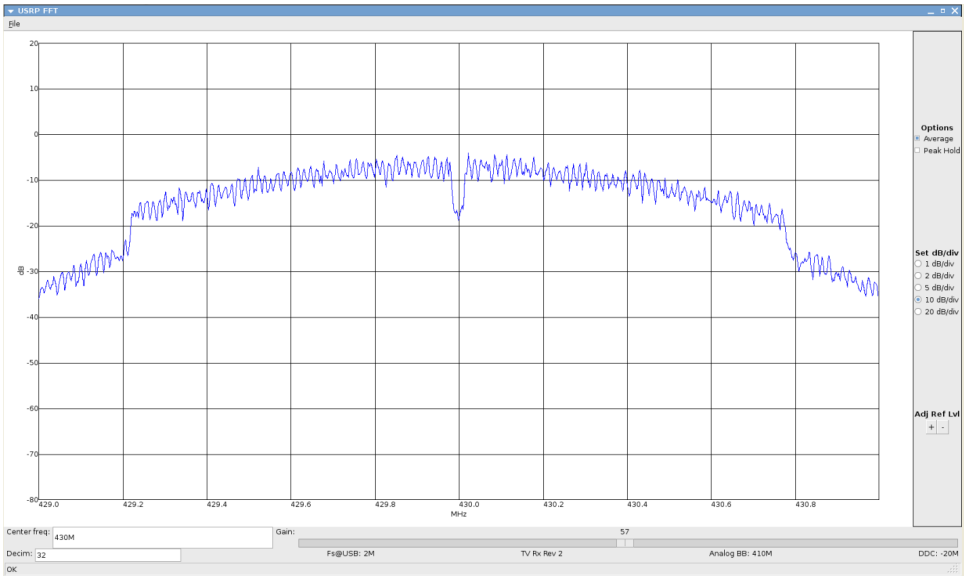

Figure 4.7: Adaptive Interference Avoidance CR Demonstration - Contiguous Multi-carrier Transmission

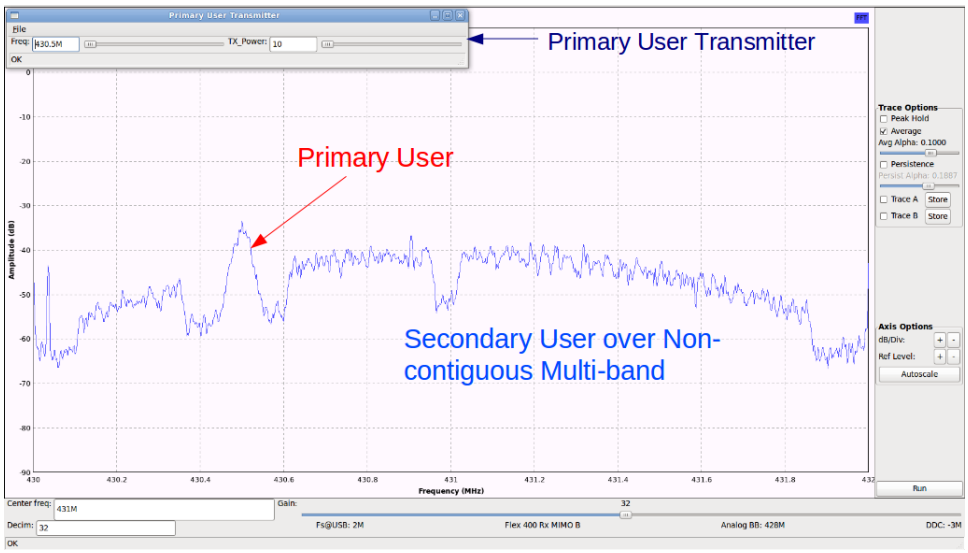

Figure 4.8: Adaptive Interference Avoidance CR Demonstration - Non-Contiguous Multi-carrier Transmission 1

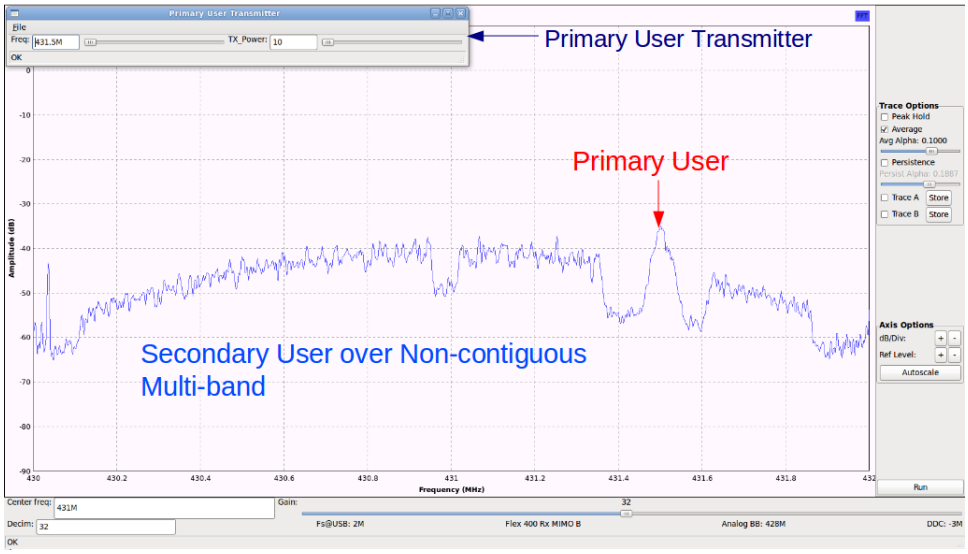

Figure 4.9: Adaptive Interference Avoidance CR Demonstration - Non-Contiguous Multi-carrier Transmission 2

Fig. 4.10 shows the setup of the interference avoidance cognitive radio. As can be seen on the two laptop screens, real time video and audio transmission over the cognitive link is supported seamlessly.

Fig. 4.11, Fig. 4.12, and Fig. 4.13 illustrate the spectrum of contiguous and non-contiguous multi-carrier waveforms captured by Agilent spectrum analyzer,

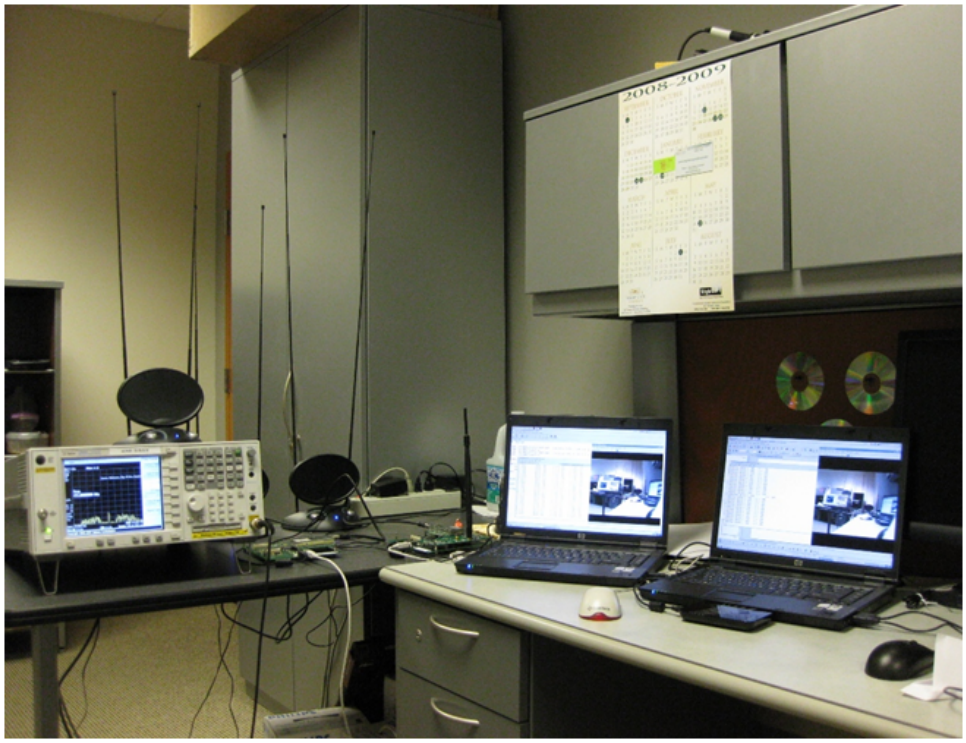

Figure 4.10: CR Demonstration

confirming the effectiveness of our overlay waveform transmission. Fig. 4.13 shows the cognitive radio taking advantage of transmitting multiple spectrum holes by utilizing multiple non-contiguous spectrum bands.

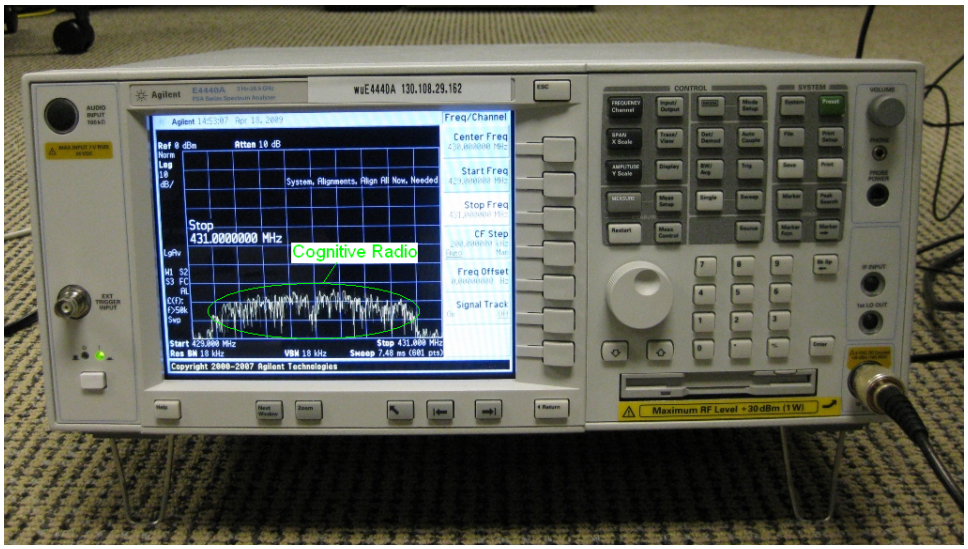

Figure 4.11: Contiguous Multi-carrier Transmission Spectrum Observed by Spectrum Analyzer

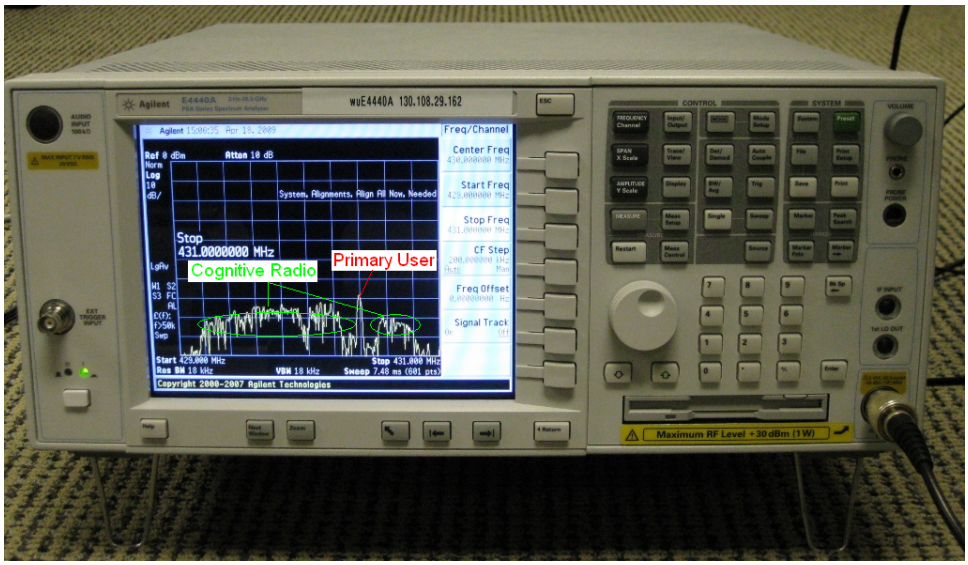

Figure 4.12: Non-Contiguous Multi-carrier Transmission Spectrum Observed by Spectrum Analyzer - 1 Primary User

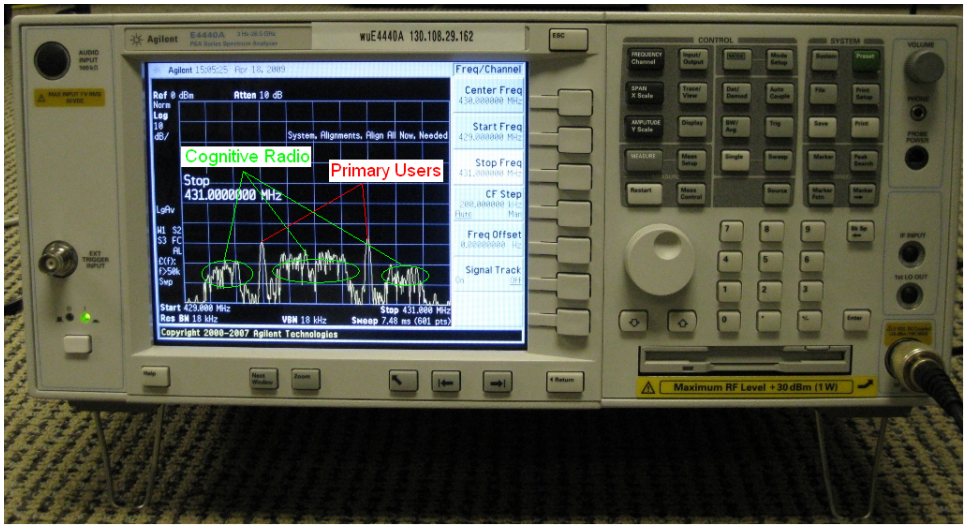

Figure 4.13: Non-Contiguous Multi-carrier Transmission Spectrum Observed by Spectrum Analyzer - 2 Primary Users

4.5 SMSE-based Overlay CR with Spectrum Mobility Feature Demonstration

Spectrum mobility [59] is the process that a secondary based CR user changes its operation frequency, uses the spectrum in a dynamic manner by allowing the CR to operate in the best vacant band, and maintains seamless communication during the transition to a better band.

In Chapter 4.4, the SMSE-based intelligent interference avoidance CR has been demonstrated. However, if the PU_TX transmits a wide band signal, for example a signal with 2MHz bandwidth, there is not enough spectrum available for SU. Hence, SU will perform spectrum mobility feature to switch to the next available spectrum hole. In this section, we demonstrate the spectrum mobility over SMSE based overlay CR via GNU SDR and USRP. The block diagram of frequency mobility demonstration is shown in Fig. 4.4.

Fig. 4.14 illustrates how the SU_TX works. Going through the ADC and DDC on the USRP, digitized data are collected and fed to the spectrum sensing engine. All the activated TV channels and other transmissions can be detected, as well as all the 'white spaces'. SU_TX will select a better band which is relatively far away from the primary users, and communicate with SU_RX. To avoid huge size of collected digitized data, the spectrum sensing engine applies packet based sensing algorithm. The spectrum sensing engine senses the environment when every 200 packets are transmitted. If no PU is sensed reactive, SU stays on the current band to communicate. If a PU is reactive, the sensing engine analyzes it further to decide that it is a narrow band PU (PU_NB) or a wide band PU (PU_WB). If a PU_NB is active, the corresponding subcarriers are turned off to avoid any interference from and to the PU_NB, which we have demonstrated in section 4.4. If a PU_WB is active, the SU_TX changes to the next available band. Then, a control signal is

sent out to inform the SU_RX. Meanwhile, SU_TX adapts itself to the new band to transmit the real-time video. After SU changing to a new band, if other PU_NB is active, SU still has the ability to dynamically turn off the subcarriers which are occupied by the PU_NB. All the PUs and SU coexist without interference from and to each other.

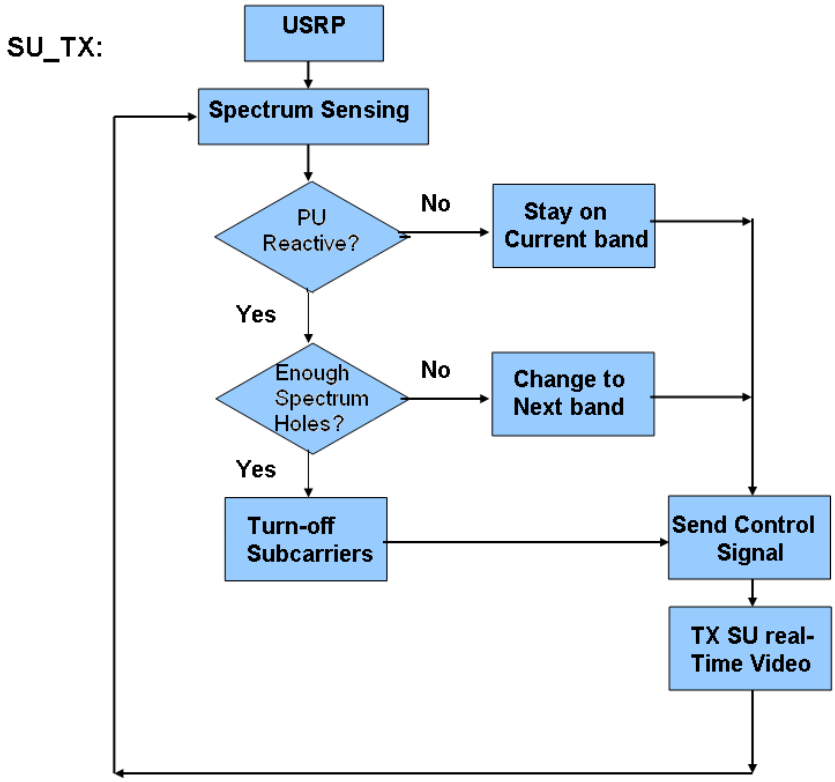

Figure 4.14: Secondary User Transmission State Diagram

Fig. 4.15 illustrates how SU_RX works. It is much simpler than the transmission diagram. First, SU_RX listens to the control signal. Then, it sets the reception parameters according the control signal, such as turning off the subcarriers or changing the operating frequency. Last, it adapts itself to the new environment. By experiments, 98.3% of the transmitted packets are received and 99.4% of the received packets are error-free.

Again, to validate our demonstration, we utilize Agilent Spectrum Analyzer

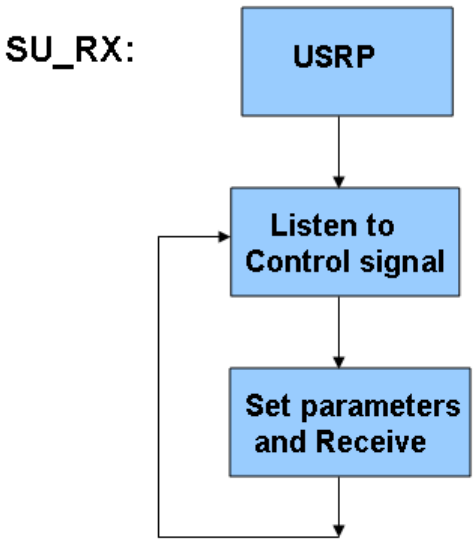

Figure 4.15: Secondary User Reception State Diagram

to capture the frequency-domain waveform during transmission. Fig. 4.16 shows the result that PU_NB is avoided. The Agilent Spectrum Analyzer screen shows a 2 MHz span. SU employs SMSE framework to generate multi-carrier transmission waveforms. The subcarriers, which are occupied by PU_NB, are turned off. Hence, SU transmits over non-contiguous spectrum holes with lower power. No interference is caused from and to PU_NB.

Fig. 4.17 demonstrates the spectrum mobility feature. The Agilent Spectrum Analyzer screen is set to 5 MHz span. We can tell from the screen that a wider PU is active. Hence, to avoid interference to each other, a better band is decided, and SU dynamically adapts into it. Again, no interference is caused from and to each other.

After SU changing to the new operating band, other PU_NB is active. The result is shown in Fig. 4.18. 5 MHz span is set on the Agilent Spectrum Analyzer screen. Two primary users are reactive in the band, the SU not only has the ability to turn off the subcarriers and operate on non-contiguous spectrum holes, it also has the ability to dynamically change the operating frequency to a better band if

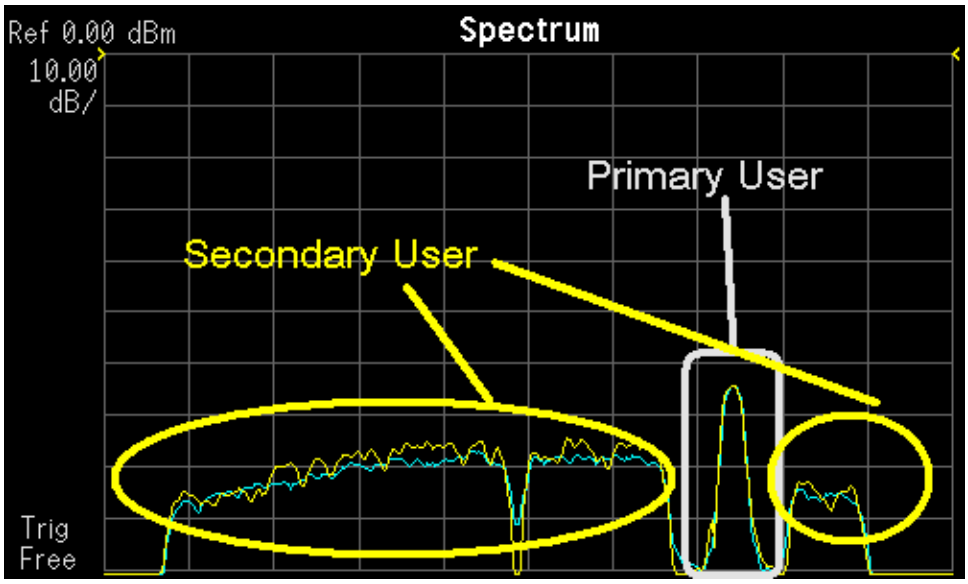

Figure 4.16: Secondary User Coexisting with Narrow Band Primary User

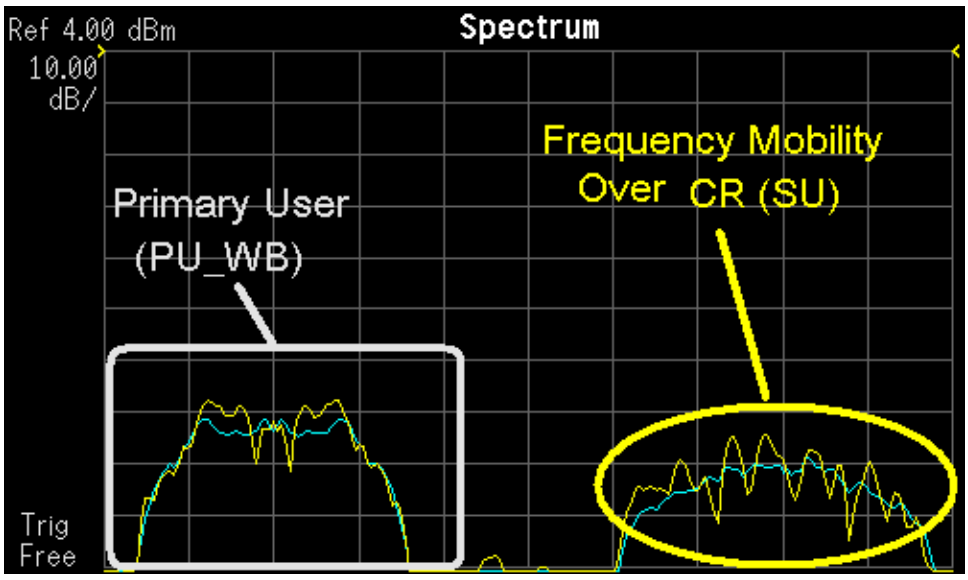

Figure 4.17: Secondary User Coexisting with Wide Band Primary User

70% of current band is occupied by the PU or the channel condition getting worse. Meanwhile, seamless communication is maintained during the transition to a better band. All the PUs and SU coexist with no interference from and to each other.

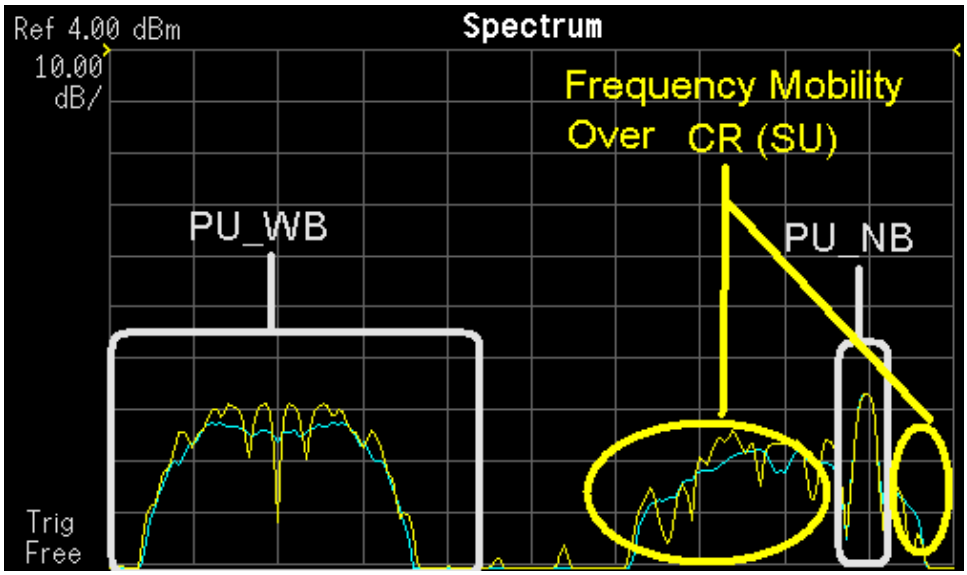

Figure 4.18: Secondary User Coexisting with Wide Band and Narrow Band Primary User

4.6 Conclusion

In this chapter, an SMSE-based overlay CR with spectrum mobility feature is implemented and demonstrated via SDR. A real-time seamless video transmission is implemented and demonstrated without interference from the primary user and to the primary user. By utilizing multi-carrier technology, a multiple non-contiguous overlay waveform is generated which can take advantage of multiple spectrum holes. Through dynamically adjusting transmission parameters, a flexible, agile and robust cognitive radio node is demonstrated. Agilent spectrum analyzer confirms the effectiveness of our CR design.

SMSE-base Overlay Cognitive Radio Implementation and Demonstration in Highly Mobile Environment

5.1 Motivation

Multi-carrier transmission such as OFDM has been considered a strong candidate for next generation high-data-rate wireless communication systems [26]. However, it is not suitable for mobile communication systems due to the frequency offset introduced by Doppler shift in high mobility environment. With this frequency offset, the orthogonality among all the OFDM subcarriers is lost and intercarrier interference (ICI) is generated. This is illustrated in Fig. 5.1.

To cancel the ICI, existing methods are with their drawbacks. The BER performance after ICI cancellation is still significantly worse than the original OFDM system without ICI. More important, most of the existing ICI cancellation methods reduce the ICI and improve the BER performance at the cost of lowering the transmission rate and reducing the bandwidth efficiency.

It has been observed that the ICI coefficient matrix in OFDM is an orthogonal

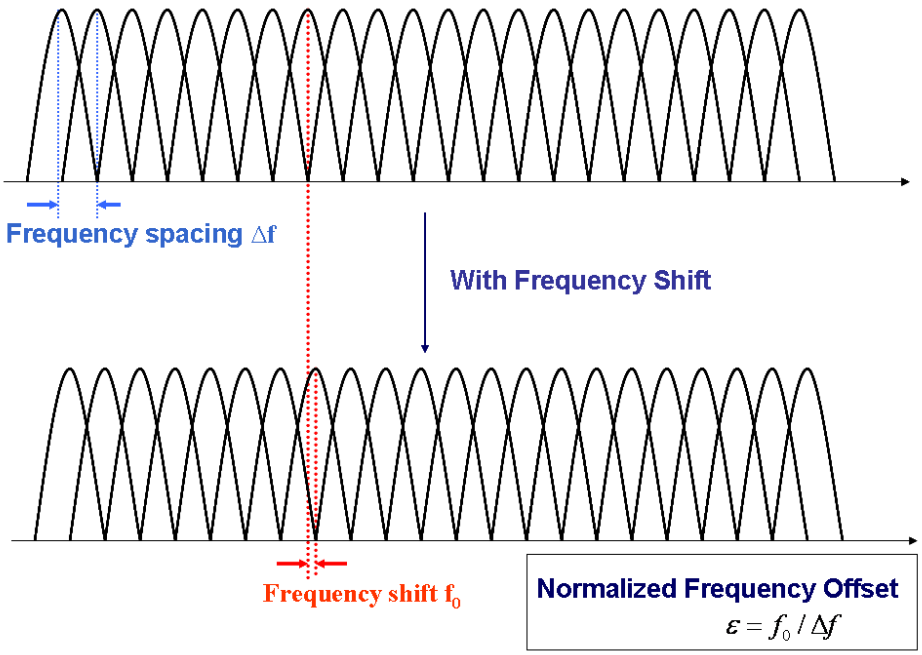

Figure 5.1: Intercarrier Interference

matrix. Hence, at the receiver side, an OFDM with ICI can be considered as a MC-CDMA system where all the N data symbols carried by the OFDM transmission are spread over all N subcarriers. However, since the frequency offset is time varying and unknown at the receiver side, the spreading code matrix of the equivalent MC-CDMA system is unknown. Hence, it has been proposed to transmit training sequences to estimate the frequency offset and cancel ICI via the estimated frequency offset. Obviously, it requires that some communication resource needs to be allocated for the training sequence.

In this chapter, we propose a brand new approach to solve the ICI problem in mobile OFDM system without estimating frequency offset through training symbols (and without reducing data rate). Specifically, we propose to quantize the normalized frequency offset into M discrete values, leading to M spreading code matrices as candidates. Next, by decoding the received signal using these M spreading code matrices, M decisions are made on the data symbols. Using these M data symbols to recreate the received signal with ICI and measuring the Euclidean

distance of the M recreated signals with the actual received signal, the best normalized frequency offset is chosen and the best corresponding data symbols are determined. Simulation results over AWGN channel and mobile multi-path fading channel demonstrate that not only the proposed system effectively eliminates ICI and offers the best BER performance available which matches the BER performance of OFDM system without ICI, it achieves the superb performance with reasonable computational complexity. It is shown that the complexity of the proposed system is linearly growing with the number of quantization levels M, and M does not have to be a big number to achieve the best performance. Simulation results show that we only need to pick $M = 10$. Last, an SMSE-base cognitive radio in highly mobile environment is implemented and demonstrated using GNU SDR and USRP platform.

5.2 ICI of OFDM Systems and Orthogonality

It is well known that the received OFDM signal on subcarrier k in AWGN channel with ICI is

$$Y(k) = X(k)S(0) + \sum_{l=0, l\neq k}^{N-1} X(l)S(l-k) + n_k, \qquad k = 0, 1, \ldots, N-1 \tag{5.1}$$

where N is the total number of the subcarriers, $X(k)$ denotes the transmitted symbol ($X(k) \in \{+1, -1\}$ if BPSK is employed, for example) for the k^{th} subcarrier, n_k is the additive Gaussian noise sample. The sequence $S(l-k)$ is the ICI coefficient between l^{th} subcarrier and k^{th} subcarrier:

$$S(l-k) = \frac{\sin(\pi(\varepsilon + l - k))}{N \sin(\frac{\pi}{N}(\varepsilon + l - k))} \cdot \exp\left(j\pi\left(1 - \frac{1}{N}\right)(\varepsilon + l - k)\right) \tag{5.2}$$

where ε is the normalized frequency offset given by $\varepsilon = \frac{f_0}{\Delta f}$, f_0 is the frequency offset, Δf is the subcarrier bandwidth of the OFDM system. It is reasonable to assume that $0 \leq \varepsilon < 1$.

Now, denote vector $\vec{X}$ as the transmitted symbol $\vec{X} = \{X(0), X(1), \ldots, X(N-1)\}$, vector $\vec{Y}$ as the received signal vector $\vec{Y} = \{Y(0), Y(1), \ldots, Y(N-1)\}$, and $\vec{n} = \{n_0, n_1, \ldots, n_{N-1}\}$, we have:

$$\vec{Y} = \vec{X}\mathbf{S} + \vec{n} \tag{5.3}$$

where $\mathbf{S}$ is the ICI coefficient matrix, and the p^{th} row and q^{th} column element of NxN matrix $\mathbf{S}$ is

$$\mathbf{S}_{p,q} = S(p-q) \tag{5.4}$$

and the matrix $\mathbf{S}$ corresponds to

$$\mathbf{S} = \begin{bmatrix} S(0) & S(-1) & \ldots & S(1-N) \\ S(1) & S(0) & \ldots & S(2-N) \\ \vdots & \vdots & \ddots & \vdots \\ S(N-1) & S(N-2) & \cdots & S(0) \end{bmatrix} \tag{5.5}$$

From equation (5.3), it is obvious that the received signal can be viewed as a MC-CDMA (multi-carrier code division multiple access) signal with N users, the k^{th} user's information symbol is $X(k)$, and the k^{th} user's spreading code is the k^{th} column of matrix $\mathbf{S}$.

Now, it is important to note that the ICI coefficient matrix $\mathbf{S}$ is an orthogonal

matrix, i.e.,

$$\mathbf{S}\mathbf{S}^{'*} = \mathbf{I} \tag{5.6}$$

where $\mathbf{S}^{'*}$ is the conjugate transpose of matrix $\mathbf{S}$ and $\mathbf{I}$ is identity matrix.

Hence, the OFDM signal with ICI at receiver side can be considered as an orthogonal MC-CDMA system with spreading code matrix $\mathbf{S}$. As a direct result, the ICI can be totally removed from the OFDM signal if we apply a matrix multiplication to the received signal vector $\vec{Y}$:

$$\vec{R} = \vec{Y}\mathbf{S}^{'*} = \vec{X} + \vec{n}\mathbf{S}^{'*} \tag{5.7}$$

Next, we can simply make decision of $\vec{X}$ based on $\vec{R}$. Since $\mathbf{S}^{'*}$ is also an orthogonal matrix, the noise vector $\vec{n}\mathbf{S}^{'*}$ in $\vec{R}$ has the same covariance matrix as that of $\vec{n}$. Hence, the entire ICI is eliminated and the BER performance would be the same as the OFDM system without ICI.

However, the problem is: the receiver does not know the spreading code matrix $\mathbf{S}$ because the normalized frequency offset ε is unknown. Hence, it has been proposed to estimate the normalized frequency offset ε through some training symbols. Obviously, it requires that some data rate be allocated for the training symbols.

5.3 Total ICI Cancellation for OFDM

We propose a total ICI cancellation scheme to eliminate ICI on mobile OFDM systems without transmitting any training symbols (and reducing data rate). While the normalized frequency offset ε is unknown to the receiver, we can quantize ε into M equally spaced values:

$$\varepsilon'_m = m \cdot \Delta\varepsilon, m = 0, 1, \ldots, M-1 \tag{5.8}$$

where $\Delta\varepsilon$ is the quantization level of normalized frequency offset, and M is the number of quantization levels:

$$\Delta\varepsilon = \frac{1}{M}, m = 0, 1, \ldots, M-1 \tag{5.9}$$

One of these M quantized ε's is the closest to the true ε.

Now, let's build M parallel branches at the receiver. Each branch uses one of the M quantized ε's to create the corresponding ICI coefficient matrix $\tilde{\mathbf{S}}$. Hence, we have M ICI coefficient matrices $\tilde{\mathbf{S}}_0, \tilde{\mathbf{S}}_1, \ldots, \tilde{\mathbf{S}}_{M-1}$ where the m^{th} matrix corresponds to:

$$\tilde{\mathbf{S}}_\mathbf{m} = \begin{bmatrix} S_m(0) & S_m(-1) & \ldots & S_m(1-N) \\ S_m(1) & S_m(0) & \ldots & S_m(2-N) \\ \vdots & \vdots & \ddots & \vdots \\ S_m(N-1) & S_m(N-2) & \cdots & S_m(0) \end{bmatrix} \tag{5.10}$$

and

$$S_m(l-k) = \frac{\sin(\pi(\varepsilon'_m + l - k))}{N \sin(\frac{\pi}{N}(\varepsilon'_m + l - k))} \cdot \exp\left(j\pi\left(1 - \frac{1}{N}\right)(\varepsilon'_m + l - k)\right) \tag{5.11}$$

Using these M matrices, we can have M decisions on the transmitted data vector $\vec{X}$ where the m^{th} branch will make decision on the estimation of $\vec{X}$ as:

$$\hat{\vec{X}}_m = \text{sgn}\{\vec{Y}\tilde{\mathbf{S}}'^*_\mathbf{m}\} \tag{5.12}$$

where sgn(X) presents the sign of X.

Next, with the data vector estimation $\hat{\vec{X}}_m$, each branch can reproduce the received signal $\hat{\vec{Y}}_m$ by using the data vector estimation $\hat{\vec{X}}_m$, the ICI coefficient matrix of that branch $\tilde{\mathbf{S}}_\mathbf{m}$:

$$\hat{\vec{Y}}_m = \hat{\vec{X}}_m \tilde{\mathbf{S}}_\mathbf{m} \tag{5.13}$$

It is easy to understand that the one branch whose ε'_m is the closest to the true value of ε should reproduce the received signal $\hat{\vec{Y}}_m$ also closest to the received signal vector $\vec{Y}$. Hence, we only need to calculate and compare the Euclidean distances between the M reproduced received signal vectors $\hat{\vec{Y}}_m$ and the truly received signal vector $\vec{Y}$ and pick the one with the minimum distance to be the best branch and use that branch's estimated data vector as the final decision:

$$\hat{\vec{X}} = argmin\{||\hat{\vec{Y}}_m - \vec{Y}||^2\} \tag{5.14}$$

where $||\hat{\vec{Y}}_m - \vec{Y}||^2$ represents the Euclidean distance between vector $\hat{\vec{Y}}_m$ and vector $\vec{Y}$.

It is important to note that the complexity of the proposed total ICI cancellation method is linearly growing with the quantization level M, keeping the computational complexity at reasonable range. For each OFDM symbol, the total ICI cancellation scheme requires $2M$ matrix multiplications and M comparisons. The increased complexity is not significant, especially when M is small. As we will show in the next Section, we don't need to use a huge M to achieve the best performance. In all the cases, $M = 8$ is good enough to provide perfect ICI cancellation and superb BER performance matching the lower bound.

The block diagram of the proposed total ICI cancellation scheme is shown in Figure 5.2.

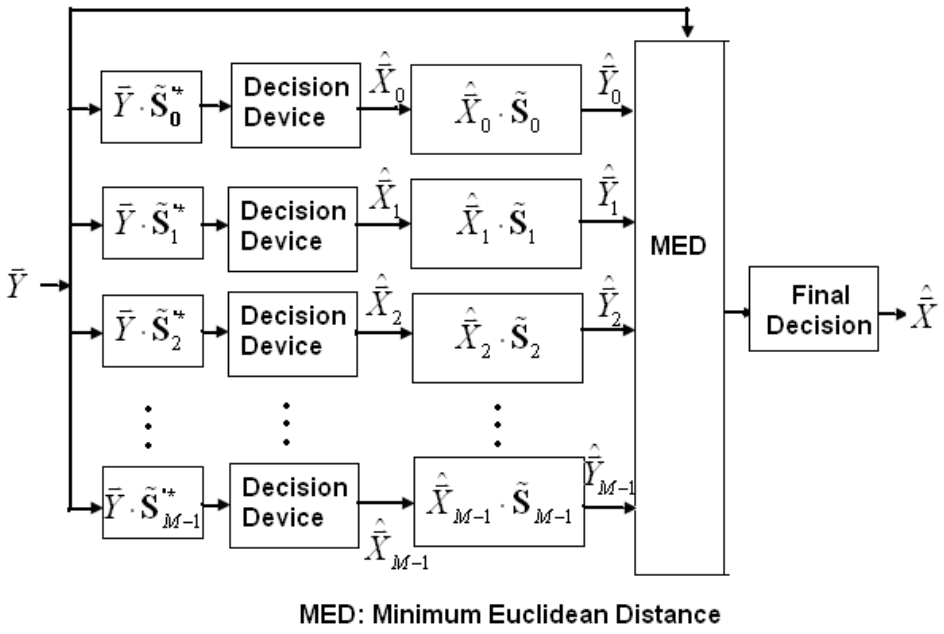

Figure 5.2: Block Diagram of the Total ICI Cancellation

5.3.1 Analysis in Multipath Fading Channels

In a multipath fading channel, let's denote the complex fading gain on the k^{th} subcarrier is α_k. Then the received OFDM signal after transmission through such a fading channel with frequency offset is:

$$\vec{Y} = \vec{X}\alpha\mathbf{S} + \vec{n} \tag{5.15}$$

where α is a diagonal matrix $\alpha = diag\{\alpha_0, \alpha_1, \ldots, \alpha_{N-1}\}$.

Similar to the analysis in AWGN channel, the received OFDM signal represented in equation (5.15) can also be viewed as an N user MC-CDMA system with spreading code matrix $\mathbf{S}$ and the k^{th} user's data symbol is $\alpha_k X(k)$. Hence, if the spreading code matrix $\mathbf{S}$ is known, we can eliminate the ICI by multiplying $\mathbf{S}'^{*}$ to the received vector $\vec{Y}$.

So the total ICI cancellation schemes works the same way as in AWGN chan-

nel with only one exception: the fading channel characteristics α needs to be estimated at the receiver side (which is required for OFDM transmission) and the reproduced received signal vector now has to consider the fading effects:

$$\hat{\vec{Y}}_m = \hat{\vec{X}}_m \alpha \tilde{\mathbf{S}}_\mathbf{m} \tag{5.16}$$

5.4 Simulation Results

In this section, we use numerical simulation results to present the effectiveness of the proposed total ICI cancellation scheme. We provide BER simulation results for the proposed total ICI cancellation scheme in AWGN channel and multipath fading channel.All the systems are assumed to have $N = 32$ subcarriers and employ BPSK modulation.

5.4.1 AWGN Channel with a Constant Frequency Offset

The simplest way to examine the effectiveness of the proposed total ICI cancellation scheme is to transmit signals through a AWGN channel with a constant frequency offset between the transmitter and receiver. Figure 5.3 illustrates the simulation result when the normalized frequency offset (NFO) $\varepsilon = 0.1$, Figure 5.4 shows the case when $\varepsilon = 0.2$, and Figure 5.5 shows the case when $\varepsilon = 0.3$. In the total ICI cancellation scheme, we use $M = 10$. In both of the two figures, the blue line shows the BER performance of OFDM without ICI, the green line marked with circles represents the performance of OFDM with ICI, and the red line marked with stars represents that of our proposed total ICI cancellation scheme. Since we chose $M = 10$, the quantization level of normalized frequency offset $\Delta\varepsilon = 0.1$. Hence, one of the M branches actually has the perfect ICI coefficient matrix to work with.

To prove the effectiveness of our total ICI cancellation method in all scenarios, Figure 5.6 presents the results when $\varepsilon = 0.287532$ so none of the M branches matches the actual ε. It is obvious from these figures that when the normalized frequency offset ε increases, the BER performance of OFDM significantly degrades, but the total ICI cancellation scheme eliminates the ICI and provides the same BER performance as that of a OFDM without ICI.

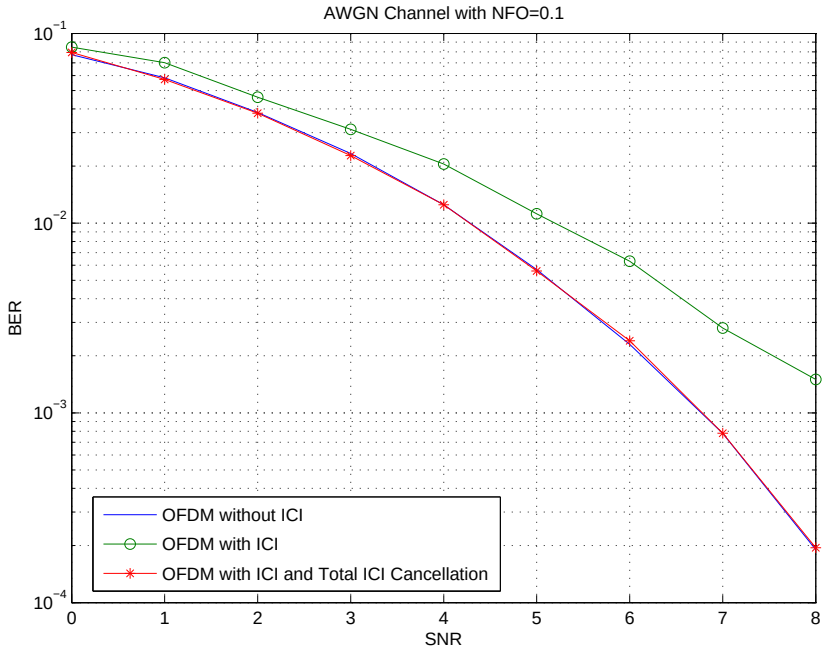

Figure 5.3: AWGN Channel with NFO=0.1

Figure 5.7 shows the BER performance versus normalized frequency offset ε. It is evident that with the increase of ε, the BER performance of OFDM significantly degrades while the OFDM with total ICI cancellation keeps the same performance despite the frequency offset.

5.4.2 Multipath Mobile Channels

In a practical mobile multipath radio channel, time-variant multipath propagation leads to Doppler frequency shift which is a random variable. Here we measure

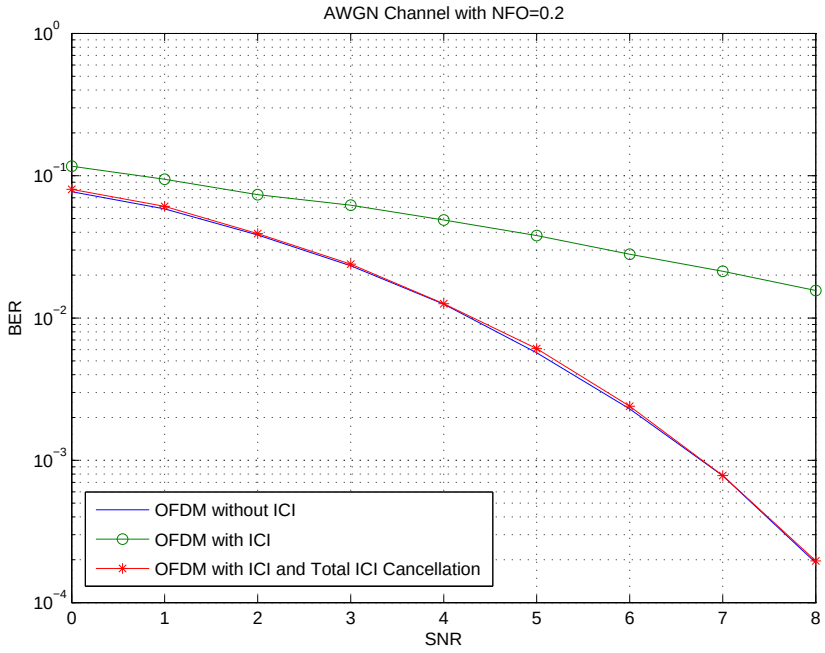

Figure 5.4: AWGN Channel with NFO=0.2

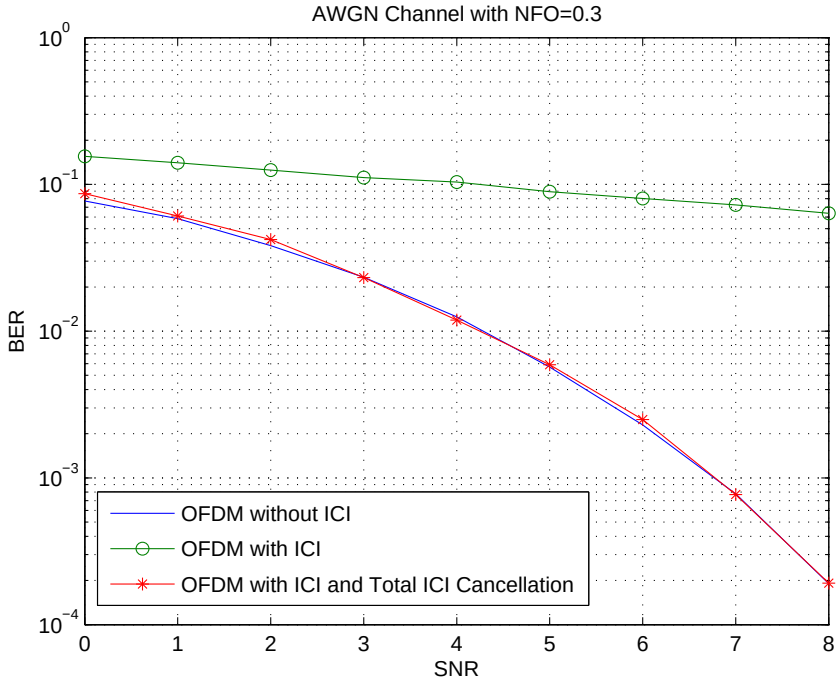

Figure 5.5: AWGN Channel with NFO=0.3

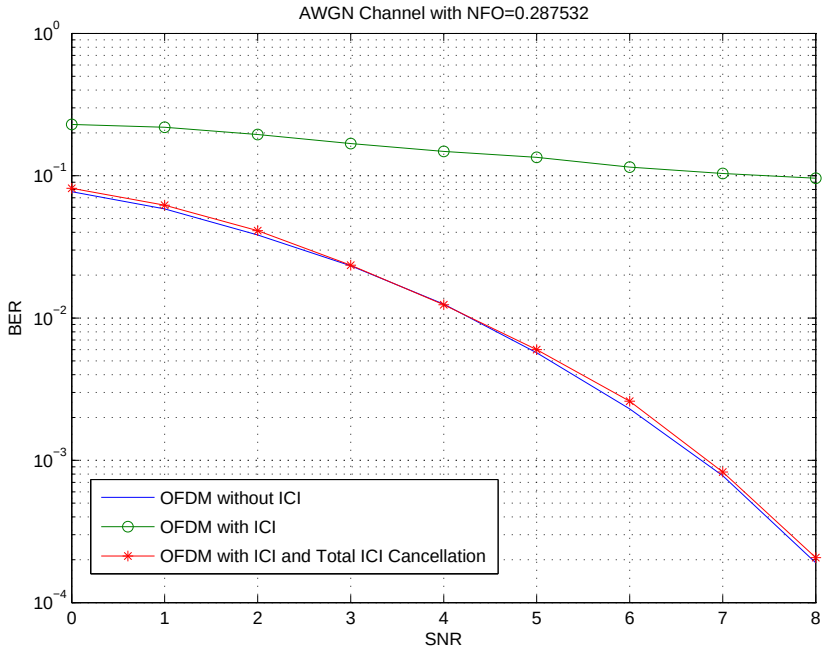

Figure 5.6: AWGN Channel with NFO=0.287532

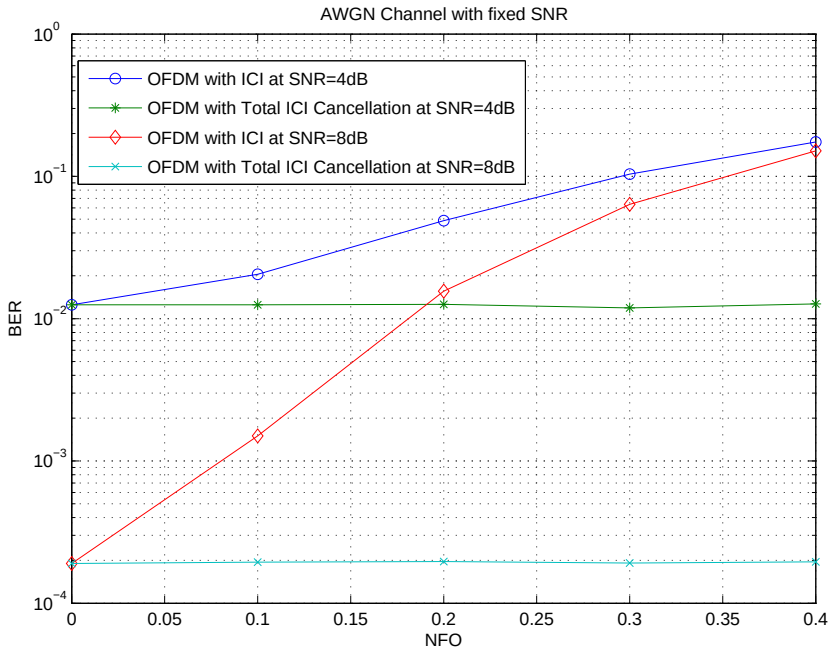

Figure 5.7: AWGN Channel with Fixed SNR

the performance of the proposed total ICI cancellation method in multipath fading channels. As a measure of Doppler frequencies, we use the normalized maximum

Doppler spread ε_B, which is defined as the ratio between the channel maximum Doppler spread to the subcarrier bandwidth. We use the Hilly Terrain (HT) channel models defined by the GSM standard as our channel model. Total number of subcarriers is also assumed to be 32.

Figure 5.8 shows the case when $\varepsilon_B = 0.1$, Figure 5.9 shows the case when $\varepsilon_B = 0.2$, and Figure 5.10 shows the case when $\varepsilon_B = 0.3$. In the total ICI cancellation scheme, we use $M = 10$. In all the figures, the blue line shows the BER performance of OFDM without ICI, the green line marked with circles represents the performance of OFDM with ICI, and the red line marked with stars represents that of our proposed total ICI cancellation scheme. Obviously, the proposed total ICI cancellation entirely eliminates the effect of ICI and matches the performance of the OFDM without ICI in fading channels as well.

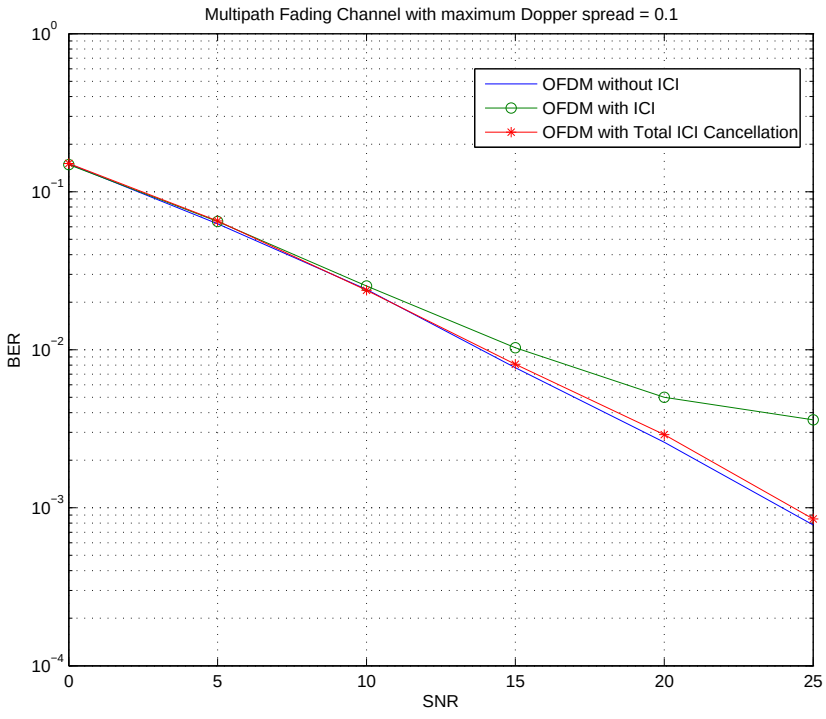

Figure 5.8: Fading Channel with Normalized Maximum Doppler Dpread = 0.1

Figure 5.11 illustrates the effect of the number of normalized frequency offset

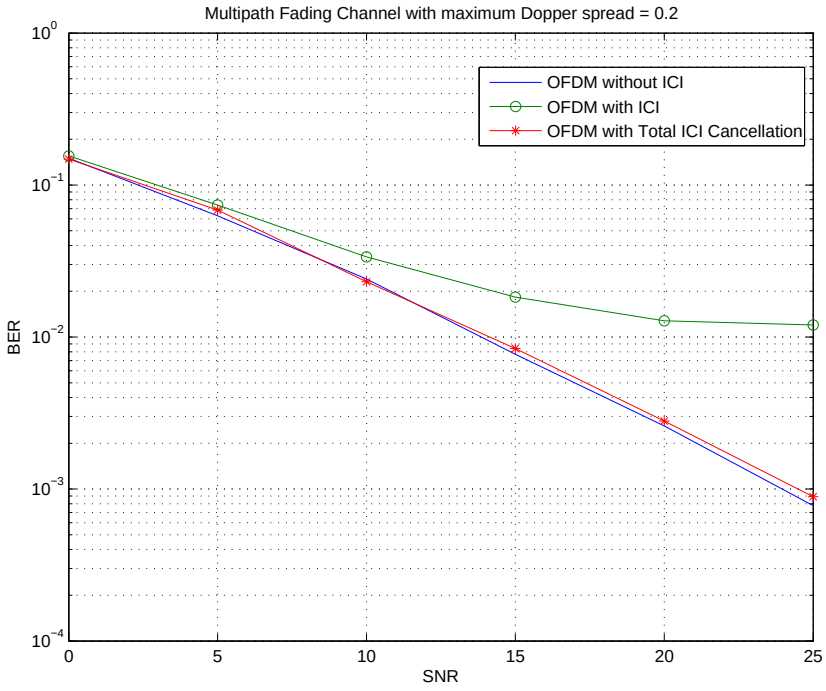

Figure 5.9: Fading Channel with Normalized Maximum Doppler Spread = 0.2

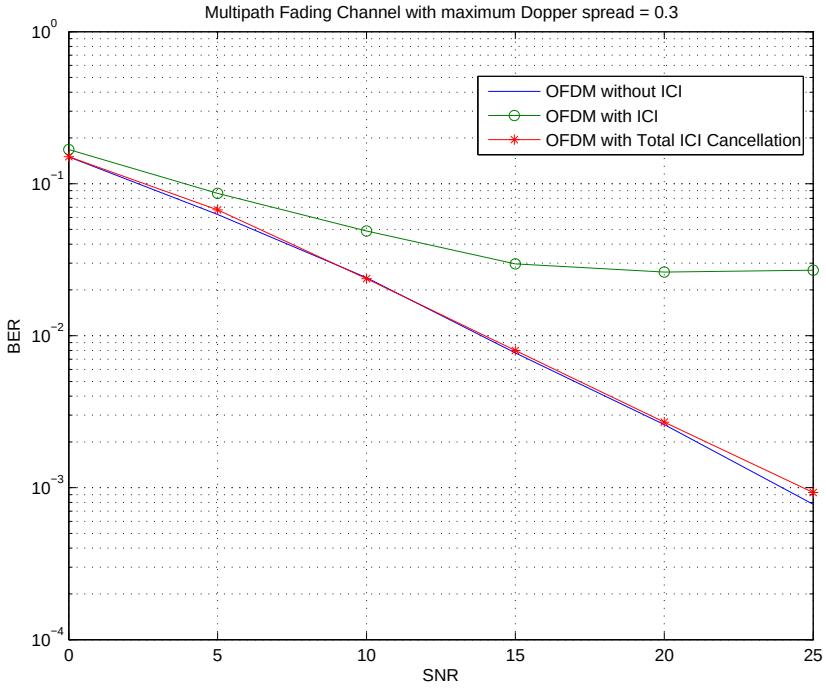

Figure 5.10: Fading Channel with Normalized Maximum Doppler Spread = 0.3

quantization levels M on the performance of the proposed total ICI cancellation scheme. In Figure 5.11, three BER versus M curves of different SNRs are shown. It is easy to understand that when M increases, more quantization levels are used and better ICI coefficient matrix estimation is achieved, so the performance of the proposed scheme will also improve. As shown in Figure 5.11, when M is very small, the proposed total ICI cancellation scheme actually offers pretty bad performance due to the large quantization error. However, when M increases, the total ICI cancellation converges fast and provide ICI cancellation and BER improvement quickly. When M is larger than 5, there is no noticeable performance gain to increase the quantization level. This can be explained as the following: when the quantization step $\Delta\varepsilon$ is small enough, the total ICI cancellation's ICI cancellation capability is enough to remove all the intercarrier interference and there is no need to decrease $\Delta\varepsilon$ anymore. It is evident from Figure 5.11 that the computational complexity of the proposed scheme is very reasonable.

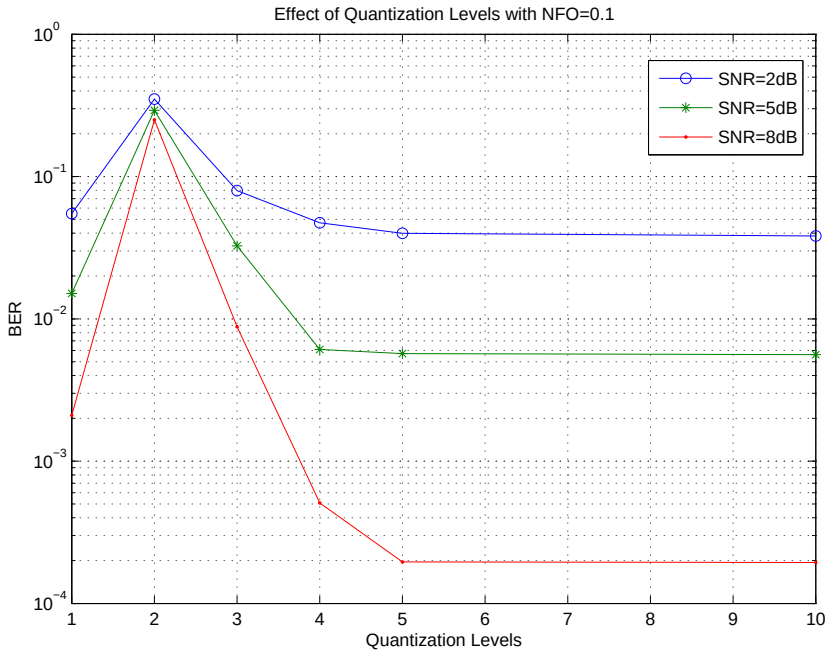

Figure 5.11: Effect of NFO Quantization Levels in AWGN Channel NFO=0.1

5.5 Demonstration via SDR

To demonstrate an adaptive interference avoidance cognitive radio in highly mobile environment, we integrate total ICI cancellation scheme onto SMSE-based intelligent interference avoidance CR, and implement an SMSE based overlay CR in highly mobile environment. Specifically, the spectrum sensing engine detects which subcarriers are occupied by the primary users. Next, by switching off those subcarriers, a non-contiguous multi-carrier transmission is performed over non-contiguous multiple spectrum bands. To perform the CR in highly mobile environment, a frequency offset is added manually onto the transmitter's center frequency. The CR receiver SU_RX applies the total ICI cancellation algorithm to remove the ICI and decode the SMSE-based waveform. The real-time video transmission is maintained.

The system block diagram of the adaptive interference avoidance CR is depicted in Fig. 5.12.

The webcam with a microphone captures the real-time video and audio signals. SU_TX senses the spectrum, finds an unoccupied band, and adapts itself into the environment. Next, we employ a control channel to inform the receiver important parameters necessary to decode the data. Such parameters include center frequency, total number of subcarriers, subcarriers to be tuned off, etc. Last, we employ SMSE waveform generator to generate contiguous multi-carrier waveform, as well as the non-contiguous multi-carrier waveform to carry the real-time seamless video data. It is reasonable to use package based sensing algorithm. SU_TX senses the spectrum when every 200 packages are transmitted. If there is any primary user becoming active in the band, SU_TX adapts to the environment quickly, and turns off the subcarrier that are occupied by narrowband emission, or switches to the next available spectrum hole.

Because this SMSE based overlay CR is in a highly mobile environment, we

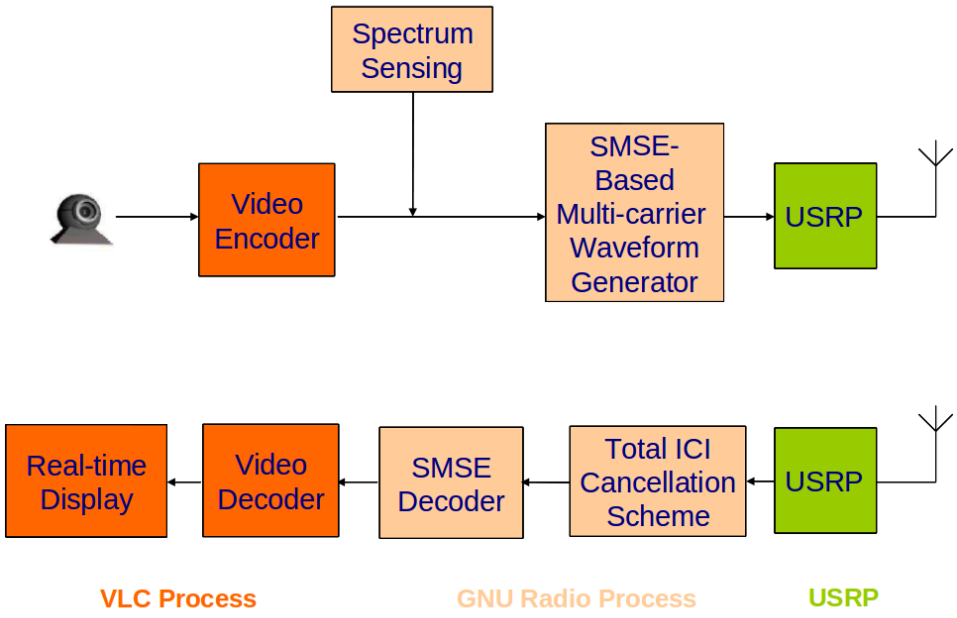

Figure 5.12: SMSE Based Overlay CR in Highly Mobile Environment Block Diagram

employ the total ICI cancellation scheme at the demodulation side. By calculating and comparing the Euclidean distances between the M reproduced received signal vectors and the truly received signal vector, the best branch is chosen, meanwhile, that branch's estimated data vector is utilized as the final decision. Then, the demodulated data are fed into the VLC video decoder and played in real-time.

For this demonstration, the total transmission bandwidth is 2MHz. The total number of subcarriers is 64. Hence, the frequency separation between adjacent subcarriers is $\Delta f = 2M/64 = 0.03125MHz$. Fig. 5.13 is the spectrum captured by USRP, centered at 515MHz with 2MHz bandwidth. The spectrum in red is the one without frequency offset. The spectrum in blue is the one with frequency offset. Fig. 5.14 and Fig. 5.15 are spectrum captured by USRP, which demonstrate that PU and SU coexist without and with frequency offset, respectively. Obviously, the receiver needs to eliminate this frequency offset to perfectly demodulate the data.

We have conducted thorough test and experiments on the performance of our

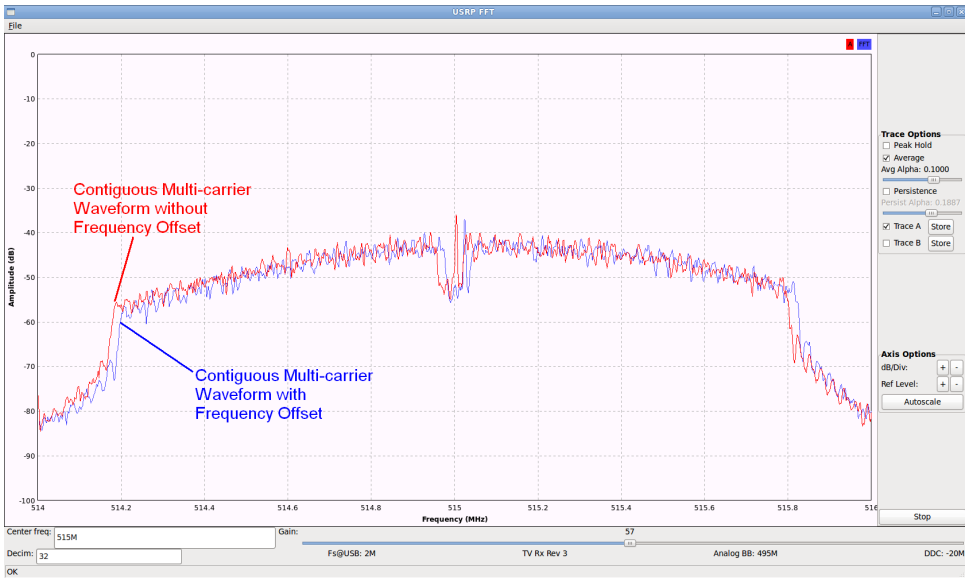

Figure 5.13: Spectrum Comparison with and without Frequency Offset, Captured by USRP

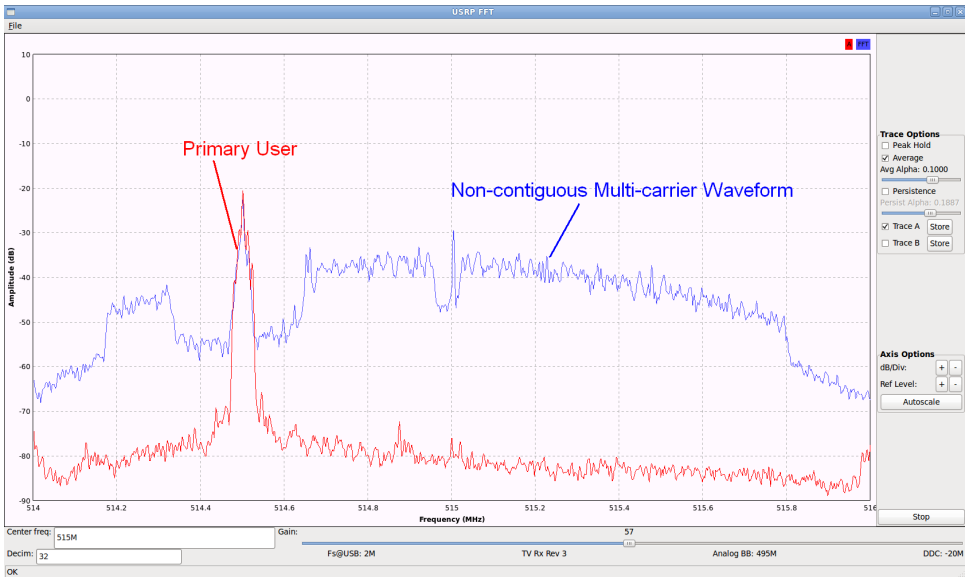

Figure 5.14: PU and SU Coexisting without ICI, Captured by USRP

demonstration for both static and mobile environments. In static environment where no mobility and no ICI is involved, 98.13% of the transmitted packets are successfully received and 99.4% of the received packets are errorless. When mobility and ICI are introduced, no package can be received. After total ICI cancellation scheme is applied, 98.1% of the transmitted packets are received and 99.26% of the

Figure 5.15: PU and SU Coexisting with ICI, Captured by USRP

received packets are errorless. This vividly proves the effectiveness of the total ICI cancellation scheme.

Figure 5.16: CR Demonstration

Fig. 5.16 shows the setup of this SMSE based overlay CR. As can be seen on

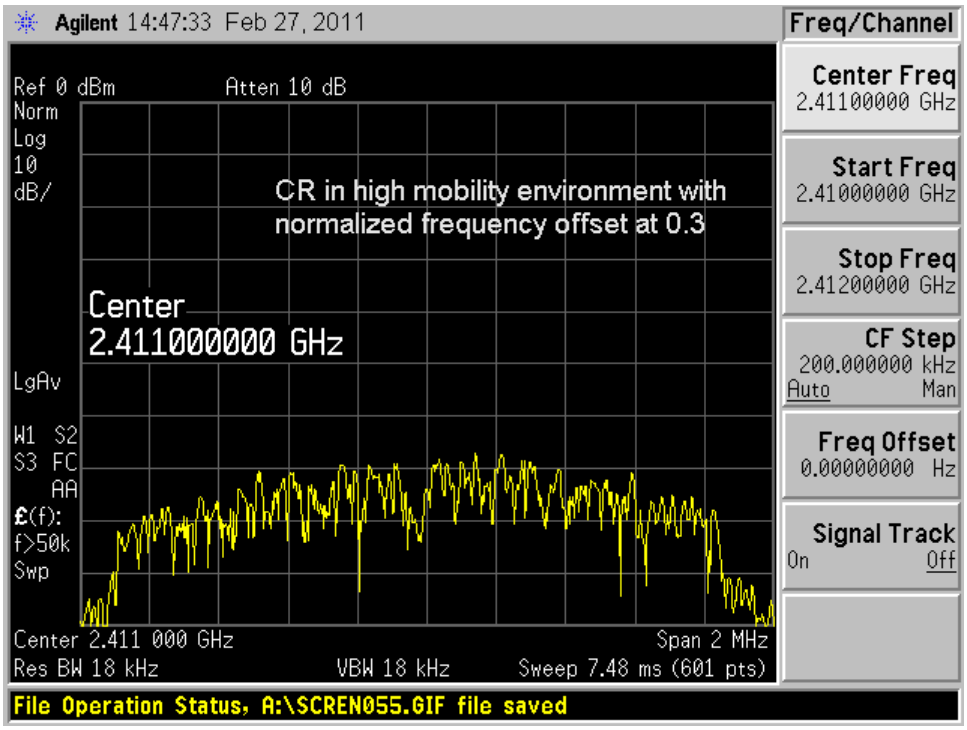

Figure 5.17: SMSE-based Cognitive Radio in Highly Mobile Environment, Captured by Agilent Spectrum Analyzer

the two laptop screens, real-time video and audio transmission over the cognitive link is supported seamlessly.

The beauty of employing GNU radio and USRP as the software platform and hardware solution is making a flexible, agile, and robust cognitive radio node. To validate the transmission, we also employ RFX2400 and Agilent Spectrum Analyzer. Fig. 5.17, captured by Agilent spectrum analyzer, shows the result that SU, centered at 2.411GHz, is occupying the entire 2MHz band in mobility environment with normalized frequency offset at $\epsilon = 0.3$ when no PU is active. Fig. 5.18 and Fig. 5.19 show the results that PUs are avoided in mobility environment with normalized frequency offset at $\epsilon = 0.3$. The Agilent Spectrum Analyzer screen shows a 2MHz span. SU employs SMSE framework to generate multi-carrier transmission waveforms. The subcarriers, which are occupied by PU_NB, are turned off. Hence, SU transmits over non-contiguous spectrum holes with lower power. No interfer-

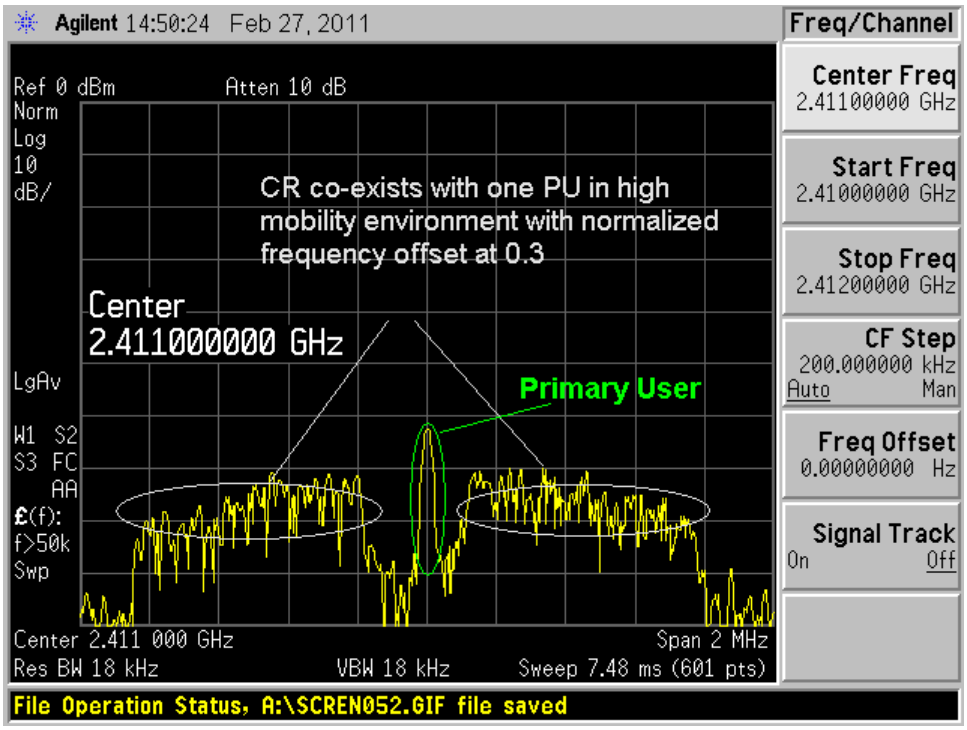

Figure 5.18: Secondary User Coexisting with one Narrow Band Primary User in Highly Mobile Environment with $\epsilon = 0.3$, Captured by Agilent Spectrum Analyzer

ence is caused from and to PU. Meanwhile, the interference caused by frequency offset is also eliminated at the receiver side, and the real-time video transmission is maintained.

5.6 Conclusion

In this chapter, we propose a novel intercarrier interference cancellation scheme called total ICI cancellation for mobile OFDM systems. Taking advantage of the orthogonality of the ICI coefficient matrix, the proposed ICI cancellation scheme can eliminate the ICI experienced in mobile OFDM systems entirely and provide significant BER improvement which matches the BER performance of OFDM system without ICI at all. The total ICI cancellation scheme (1) provides perfect perfor-

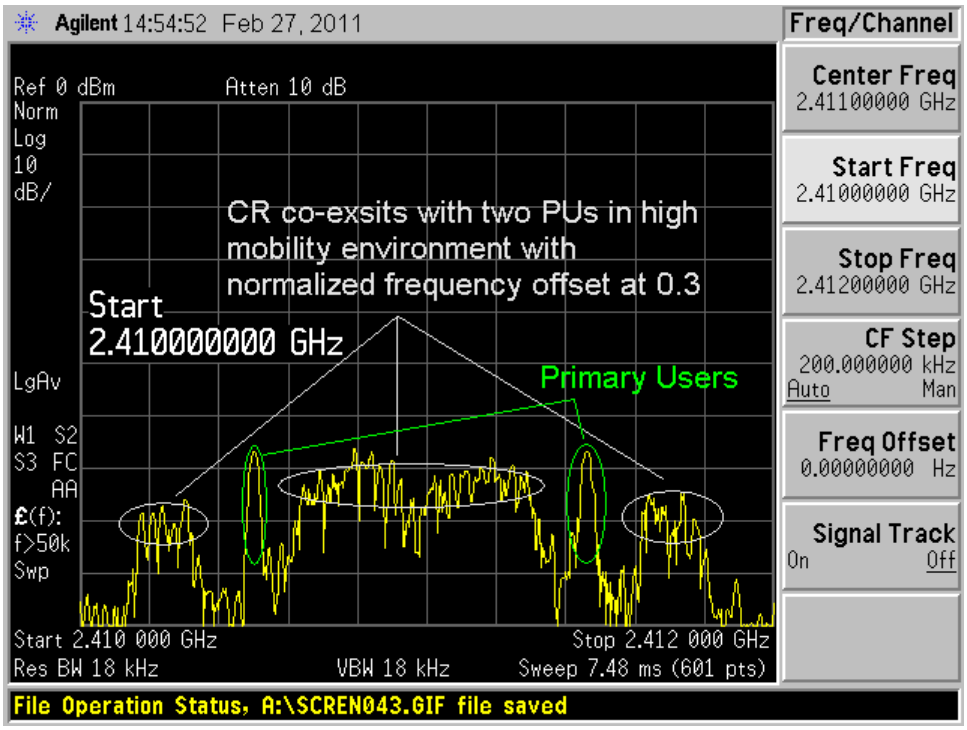

Figure 5.19: Secondary User Coexisting with Two Narrow Band Primary Users in Highly Mobile Environment with $\epsilon = 0.3$, Captured by Agilent Spectrum Analyzer

mance; (2) doesn't reduce the bandwidth efficiency of OFDM system. Simulations confirm the effectiveness of the proposed scheme, which achieves such superb performance at a very reasonable computational complexity which linearly grows with the number of normalized frequency offset quantization. More importantly, a demonstration of SMSE-based CR in high mobility environment is performed using GNU SDR and USRP platform. All the unique features of the SMSE-based CR are maintained.

Bibliography

[1] H. Arslan, *Cognitive Radio - Software Defined Radio and Adaptive Wireless Systems*. Springer-Verlag New York, LLC, 2007.

[2] P. Marchall, "Xg - next generation communications," dec. 2002. available at `http://www.darpa.mil/darpatech2002/presentations /atopdf/speeches/marshall.pdf`.

[3] Q. Zhao and B. Sadler, "A survey of dynamic spectrum access," *Signal Processing Magazine, IEEE*, vol. 24, pp. 79 –89, may 2007.

[4] J. M. III, "Cognitive radio - an integrated agent architecture for software defined radio," *Ph.D. Dissertation*, 2000.

[5] V. Chakravarthy, X. Li, Z. Wu, M. Temple, F. Garber, R. Kannan, and A. Vasilakos, "Novel overlay/underlay cognitive radio waveforms using sd-smse framework to enhance spectrum efficiency - part i: theoretical framework and analysis in awgn channel," *Communications, IEEE Transactions on*, vol. 57, pp. 3794 –3804, dec. 2009.

[6] V. Chakravarthy, X. Li, R. Zhou, Z. Wu, and M. Temple, "Novel overlay/underlay cognitive radio waveforms using sd-smse framework to enhance spec-

trum efficiency - part ii: analysis in fading channels," *Communications, IEEE Transactions on*, vol. 58, pp. 1868 –1876, jun. 2010.

[7] V. Chakravarthy, Z. Wu, M. Temple, F. Garber, and X. Li, "Cognitive radio centric overlay/underlay waveform," *New Frontiers in Dynamic Spectrum Access Networks, 2008. DySPAN 2008. 3rd IEEE Symposium on*, pp. 1 –10, oct. 2008.

[8] "Fcc frequency allocation chart," *National Telecommunications and Information Adminstration (NTIA)*, dec. 2003.

[9] V. D. Chakravarthy, "Evaluation of overlay/underlay waveform via sd-smse framework for enhancing spectrum efficiency," *Ph.D. Dissertation*, 2008.

[10] M. Roberts, M. A. Temple, M. E. Oxley, R. F. Mills, and R. A. Raines, "A general analytic framework for spectrally modulated, spectrally encoded signals," *IEEE Journal of Selected Areas on Signal Processing*, January 2007.

[11] M. Roberts, M. A. Temple, R. A. Raines, and F. Mills, "Communication waveform design using an adaptive spectrally modulated, spectrally encoded (smse) framework," *IEEE Journal of Selected Areas on Signal Processing*, June 2007.

[12] F. K. Jondral, "Software-defined radio: basics and evolution to cognitive radio," *EURASIP J. Wirel. Commun. Netw.*, vol. 2005, pp. 275–283, August 2005.

[13] J. G. Proakis, *Digital Communications*. New York: McGraw Hill, 4th ed., 2000.

[14] E. Like, V. Chakravarthy, R. Husnay, and Z. Wu, "Modulation recognition in multipath fading channels using cyclic spectral analysis," in *Global Telecommunications Conference, 2008. IEEE GLOBECOM 2008. IEEE*, pp. 1 –6, 30 2008-dec. 4 2008.

[15] D. Cabric, S. Mishra, and R. Brodersen, "Implementation issues in spectrum sensing for cognitive radios," in *Signals, Systems and Computers, 2004. Conference Record of the Thirty-Eighth Asilomar Conference on*, vol. 1, pp. 772 – 776 Vol.1, nov. 2004.

[16] R. Tandra and A. Sahai, "Fundamental limits on detection in low snr under noise uncertainty," in *Wireless Networks, Communications and Mobile Computing, 2005 International Conference on*, vol. 1, pp. 464 – 469 vol.1, june 2005.

[17] H. Tang, "Some physical layer issues of wide-band cognitive radio systems," in *New Frontiers in Dynamic Spectrum Access Networks, 2005. DySPAN 2005. 2005 First IEEE International Symposium on*, pp. 151 –159, nov. 2005.

[18] A. Sahai, R. T, S. M. Mishra, and N. Hoven, "Fundamental design tradeoffs in cognitive radio systems," in *In Proc. of the First International Workshop on Technology and Policy for Accessing Spectrum, (TAPAS*, p. 2, ACM Press, 2006.

[19] D. Cabric, A. Tkachenko, and R. Brodersen, "Spectrum sensing measurements of pilot, energy, and collaborative detection," in *Military Communications Conference, 2006. MILCOM 2006. IEEE*, pp. 1 –7, oct. 2006.

[20] S. Geirhofer, L. Tong, and B. M. Sadler, "Dynamic spectrum access in wlan channels: empirical model and its stochastic analysis," in *Proceedings of the first international workshop on Technology and policy for accessing spectrum*, TAPAS '06, (New York, NY, USA), ACM, 2006.

[21] S. Kay, *Fundamentals of Statistical Signal Prcessing: Statistical Decision Theory I*. Prentice Hall, 1998.

[22] M. Oner and F. Jondral, "Cyclostationarity based air interface recognition for software radio systems," in *Radio and Wireless Conference, 2004 IEEE*, pp. 263 – 266, sept. 2004.

[23] M. Oner and F. Jondral, "Cyclostationarity-based methods for the extraction of the channel allocation information in a spectrum pooling system," in *Radio and Wireless Conference, 2004 IEEE*, pp. 279 – 282, sept. 2004.

[24] D. Cabric and R. Brodersen, "Physical layer design issues unique to cognitive radio systems," in *Personal, Indoor and Mobile Radio Communications, 2005. PIMRC 2005. IEEE 16th International Symposium on*, vol. 2, pp. 759 –763 Vol. 2, sept. 2005.

[25] A. Fehske, J. Gaeddert, and J. Reed, "A new approach to signal classification using spectral correlation and neural networks," in *New Frontiers in Dynamic Spectrum Access Networks, 2005. DySPAN 2005. 2005 First IEEE International Symposium on*, pp. 144 –150, nov. 2005.

[26] W. Zou and Y. Wu, "Cofdm: an overview," *Broadcasting, IEEE Transactions on*, vol. 41, pp. 1 –8, mar 1995.

[27] X. Cai and G. B. Giannakis, "Bounding performance and suppressing intercarrier interference in wireless mobile ofdm," *IEEE Transactions on Communications*, vol. 51, pp. 2047–2056, December 2003.

[28] H. Minn, P. Tarasak, and V. Bhargava, "Ofdm frequency offset estimation based on blue principle," *IEEE Vehicular Technology Conference*, vol. 2, pp. 1230 – 1234, September 2002.

[29] A. J. Coulson, "Maximum likelihood synchronization for ofdm using a pilot symbol: analysis," *IEEE Journal on Selected Areas in Communications*, vol. 19, no. 12, pp. 2495 – 2503, 2001.

[30] Y. Yao and G. B. Giannakis, "Blind carrier frequency offset estimation in siso, mimo, and multiuser ofdm systems," *IEEE Transactions on Communications*, vol. 53, pp. 173–183, Jan. 2005.

[31] L. Wu, X.-D. Zhang, P.-S. Li, and Y.-T. Su, "A blind cfo estimator based on smoothing power spectrum for ofdm systems," *IEEE Transactions on Communications*, vol. 57, pp. 1924–1927, July 2009.

[32] F. Yang, K. H. Li, and K. C. Teh, "A carrier frequency offset estimator with minimum output variance for ofdm systems," *IEEE Communications Letters*, vol. 8, pp. 677–679, Nov. 2004.

[33] Y. Zhao and S.-G. Haggman, "Intercarrier interference self-cancellation scheme for ofdm mobile communication systems," *IEEE Transactions on Communications*, vol. 49, pp. 1185–1191, July 2001.

[34] A. Seyedi and G. J. Saulnier, "General ici self-cancellation scheme for ofdm systems," *IEEE Transactions on Vehicular Technology*, vol. 54, pp. 198–210, Janurary 2005.

[35] H.-G. Ryu, Y. Li, and J.-S. Park, "An improved ici reduction method in ofdm communication system," *IEEE Transactions on Boradcasting*, vol. 51, pp. 395–400, September 2005.

[36] T. W. Rondeau, "Application of artificial intelligence to wireless communications," *Ph.D. Dissertation*, 2007.

[37] G. Radio available at `http://www.gnuradio.org`.

[38] J. Crols and M. Steyaert, "Low-if topologies for high-performance analog front ends of fully integrated receivers," *Circuits and Systems II: Analog and Digital Signal Processing, IEEE Transactions on*, vol. 45, pp. 269 –282, mar 1998.

[39] A. A. Abidi, "Direct-conversion radio transceivers for digital communications," *IEEE Journal of Solid-state Circuits*, vol. 30, pp. 1399 – 1410, December 1995.

[40] B. Le, T. W. Rondeau, J. H. Reed, and C. W. Bostian, "Analog-to-digital converters: A review of the past, present, and future," *IEEE Sig. Proc. Mag.*, vol. 22, pp. 69–77, November 2005.

[41] E. Blossom, "Gnu radio: Tools for exploring the rf spectrum," *Linux Journal*, June 2004.

[42] M. Pilgrim, "Dive into python," 2004. available at http://diveintopython.org/.

[43] N. Shankar, C. Cordeiro, and K. Challapali, "Spectrum agile radios: utilization and sensing architectures," in *New Frontiers in Dynamic Spectrum Access Networks, 2005. DySPAN 2005. 2005 First IEEE International Symposium on*, pp. 160 –169, nov. 2005.

[44] S. Geirhofer, L. Tong, and B. Sadler, "A measurement-based model for dynamic spectrum access in wlan channels," in *Military Communications Conference, 2006. MILCOM 2006. IEEE*, pp. 1 –7, oct. 2006.

[45] E. Like, V. D. Chakravarthy, P. Ratazzi, and Z. Wu, "Modulation recognition in multipath fading channels using cyclic spectral analysis," *EURASIP Journal on Wireless Communications and Networking*, vol. 2009, 2009.

[46] USRP available at `http://www.ettus.com`.

[47] K. Po and J. Takada, "Signal detectino for analog and digital tv signals for cognitive radio," *IEICE Technical Report*, pp. 151–159, November 2006.

[48] W. A. Gardner, *Cyclostationarity in Communications and Signal Processing*. IEEE Press,Piscataway, NJ, USA, 1993.

[49] W. A. Gardner, "Signal interception: A unifying theoretical framework for feature detection," *IEEE Transactions on Communications*, 1988.

[50] T. O'Shea, T. Clancy, and H. Ebeid, "Practical signal detection and classification in gnuradio," *SDR Forum Technical Conference*, November 2007.

[51] F. J. Harris, "On the use of windows for harmonic analysis with discrete fourier transform," *Proceedings of the IEEE*, vol. 66, Jan. 1978.

[52] "Gsm band," available at http://en.wikipedia.org/wiki/GSM_frequency_bands#GSM_frequency_usage_in_the_Americas.

[53] "Comparison table," available at http://en.wikipedia.org/wiki/Spectral_efficiency#Comparison_table.

[54] Tektronix available at http://www.tek.com.

[55] S. W. C. Emulator available at http://www.spirent.com/Solutions-Directory/SR5500.aspx.

[56] D. Harvatin and R. Ziemer, "Orthogonal frequency division multiplexing performance in delay and doppler spread channels," *Proc. IEEE Veh. Technol. Conf.*, May 1997.

[57] V. Chakravarthy, A. Shaw, M. Temple, and A. Nunez, "Tdcs, ofdm, and mc-cdma: A brief tutorial," *IEEE Communications Magazine*, pp. s11–s16, September 2005.

[58] T. M. Schmidl and D. C. Cox, "Robust frequency and timing synchronization for ofdm," *IEEE Trans. Communications*, 1997.

[59] I. F. Akyildiz, W.-Y. Lee, M. C. Vuran, and S. Mohanty, "Next generation/dynamic spectrum access/cognitive radio wireless networks: A survey," *COMPUTER NETWORKS JOURNAL (ELSEVIER*, vol. 50, pp. 2127–2159, 2006.